Complement C5a induces renal injury in diabetic kidney disease via disruption in mitochondrial metabolic agility

Journal:	*Diabetes*
Manuscript ID	DB19-0043.R2
Manuscript Type:	Original Article: Complications
Date Submitted by the Author:	08-Sep-2019
Complete List of Authors:	Tan, Sih Min; Monash University, Central Clinical School Ziemann, Mark; Deakin University - Geelong Waterfront Campus Thallas-Bonke, Vicki; Alfred Health Snelson, Matthew; Monash University, Central Clinical School Kumar, Vinod; University of Queensland Laskowski, Adrienne; Monash University, Central Clinical School Nguyen, Tuong-Vi; Baker Heart Research Institute - BHRI Huynh, Kevin; Baker Heart Research Institute - BHRI Milne, Michele; Austin Health Libianto, Renata; Monash University Baker, Scott; University of Melbourne , Endocrine Centre / Medicine Skene, Alison; Austin Health Power, David; Austin Hospital, Nephrology; MacIsaac, Richard; University of Melbourne, Encocrinology; Henstridge, Darren; Baker IDI Heart and Diabetes Institute wetsel, rick; University of Texas-Houston El-Osta, Sam; Monash University, Epigenetics in Human Health and Disease Laboratory; Meikle, Peter; Baker IDI Heart and Diabetes Institute Wilson, Scott; Alfred Health Forbes, Josephine; Mater Research Institute - UQ, Translational Research Insitute; University of Queensland , School of Medicine Cooper, Mark; Monash University Central Clinical School Ekinci, Elif; Austin Health, Endocrinology; University of Melbourne, Department of Medicine Woodruff, Trent; University of Queensland , School of Medicine Coughlan, Melinda; Monash University, Central Clinical School;

Complement C5a induces renal injury in diabetic kidney disease via disruption in mitochondrial metabolic agility

Authors: Sih Min Tan[1]*, Mark Ziemann[1,2], Vicki Thallas-Bonke[1], Matthew Snelson[1], Vinod Kumar[3], Adrienne Laskowski[1], Tuong-Vi Nguyen[4], Kevin Huynh[4], Michele V Clarke[5,6], Renata Libianto[6], Scott T Baker[5], Alison Skene[7], David A Power[6,8], Richard J MacIsaac[6,9], Darren C Henstridge[4], Rick A Wetsel[10], Assam El-Osta[1], Peter J Meikle[4], Scott G Wilson[4,11], Josephine M Forbes[12], Mark E Cooper[1], Elif I Ekinci[5,6], Trent M Woodruff[3], Melinda T Coughlan[1,4]*.

Affiliations:

[1]Department of Diabetes, Central Clinical School, Alfred Medical Research and Education Precinct, Monash University, Melbourne, Victoria, Australia.

[2]Deakin University, School of Life and Environmental Sciences, Geelong, Victoria, Australia.

[3]School of Biomedical Sciences, University of Queensland, Brisbane, Queensland, Australia.

[4]Baker Heart & Diabetes Institute, Melbourne, Australia

[5]Department of Endocrinology, Austin Health, Melbourne, Victoria, Australia.

[6]Department of Medicine, University of Melbourne, Melbourne, Victoria, Australia.

[7]Department of Anatomical Pathology, Austin Health, Melbourne, Victoria, Australia.

[8]Department of Nephrology and Institute for Breathing and Sleep, Austin Health, Melbourne, Victoria, Australia.

[9]Department of Endocrinology & Diabetes, St Vincent's Hospital, Melbourne, Victoria, Australia.

[10]Research Center for Immunology and Autoimmune Diseases, Institute of Molecular Medicine for the Prevention of Human Diseases, University of Texas-Houston, Houston, TX, USA.

[11]Department of Renal Medicine, Alfred Health, Melbourne, Victoria, Australia.

[12]Glycation and Diabetes Group, Mater Research Institute-The University of Queensland, Translational Research Institute, Woolloongabba, Queensland, Australia.

Running title: C5aR1 inhibition attenuates DKD

Word count for abstract: 240

Word count for text: 5906

Number of tables: 2

Number of figures: 6

*To whom correspondence should be addressed:

Department of Diabetes, Central Clinical School, Monash University, 99 Commercial Road, Melbourne, Victoria, Australia, Telephone: +613 99030005

Email: melinda.coughlan@monash.edu

sihmin.tan@monash.edu

Tweet:

@MelindaCoughlan @sihmin_tan @CCSMonash @MonashDiabetes

A new immunometabolic pathway uncovered in diabetes! Innate immune Complement C5a induces kidney injury in diabetes by disrupted mitochondrial agility.

#diabetes #kidney #mitochondria #complement #immunometabolism

Figure 6 best summarizes the article

Abstract

The sequelae of diabetes mellitus include microvascular complications such as diabetic kidney disease (DKD), which involves glucose-mediated renal injury that is associated with a disruption in mitochondrial metabolic agility, inflammation and fibrosis. We explored the role of the innate immune complement component C5a, a potent mediator of inflammation, in the pathogenesis of DKD in clinical and experimental diabetes. Marked systemic elevation in C5a activity was demonstrated in patients with diabetes which was not therapeutically targeted by conventional renoprotective agents. C5a and its receptor (C5aR1) were upregulated early in the disease process and prior to manifest kidney injury in several diverse rodent models of diabetes. Genetic deletion of C5aR1 in mice conferred protection against diabetes-induced renal injury. Transcriptomic profiling of kidney revealed diabetes-induced downregulation of pathways involved in mitochondrial fatty acid metabolism. Interrogation of the lipidomics signature revealed abnormal cardiolipin remodelling in the diabetic kidney, a cardinal sign of disrupted mitochondrial architecture and bioenergetics. In vivo delivery of an orally active inhibitor of C5aR1 (PMX53) reversed the phenotypic changes and normalized the renal mitochondrial fatty acid profile, cardiolipin remodelling and citric acid cycle intermediates. In vitro exposure of human renal proximal tubular epithelial cells to C5a led to altered mitochondrial respiratory function and reactive oxygen species generation. These studies provide evidence for a pivotal role of the C5a/C5aR1 axis in propagating renal injury in the development of DKD via disruption of mitochondrial agility, establishing a new immunometabolic signalling pathway in DKD.

Diabetic kidney disease (DKD), affecting up to 30% of patients with both type 1 (T1D) and type 2 diabetes (T2D), is the leading cause of end stage renal disease in Western societies (1; 2). Despite optimal conventional management with pharmacological inhibition of the renin angiotensin system (RAS), glycemic and blood pressure control, a significant proportion of patients with DKD still progress over time to end stage renal failure. Thus, the identification of new molecular pathways with opportunity for therapeutic targeting to slow, halt and/or potentially reverse DKD progression would address a major area of unmet need.

The diabetic kidney is exposed to persistent metabolic and haemodynamic stressors resulting in cellular injury and activation of the innate immune response, including the complement system (3). The complement system is a highly sophisticated network of proteins that are activated in response to invading pathogens or tissue injury. Complement homeostasis is finely balanced and when subject to states of dysregulation or hyperactivation can propagate a severe inflammatory response (4). Complement comprises three mechanistic pathways; classical, lectin and alternative, with activation of any one of these commonly converging to the production of the complement C3 and C5 convertases. These enzymes cleave complement subtrates C3 and C5 respectively, resulting in the generation of the opsonic C3b, anaphylatoxins C3a and C5a and subsequently the formation of membrane attack complex (MAC; comprising C5b-9). As the terminal effector component of complement cascade, the MAC lyses, damages, or activates target cells to drive inflammation (5). All complement activation pathways result in the formation of C5a, a potent and a major effector molecule of complement, which, via ligation with the receptor C5aR1, initiates and propagates pathology in inflammatory disease states (6). The role of the C5a-C5aR1 signalling

cascade has been implicated in a number of kidney diseases in both animal models (7-10) and humans (11), however its role in DKD-associated renal injury is poorly defined.

Here, we reported that in patients with diabetes, complement is hyperactivated in both type 1 and type 2 diabetes, and not targeted by conventional DKD trajectory modifying therapies such as RAS inhibitors. C5a was generated and C5aR1 upregulated in the kidney of several models of experimental diabetes and prior to the onset of albuminuria. Inhibition of C5aR1 via genetic deletion or pharmacological targeting with PMX53 in streptozotocin-induced diabetic mice improved albuminuria and renal injury. Interrogation of the lipidomics signature revealed abnormal cardiolipin remodelling in the diabetic kidney, a cardinal sign of disrupted mitochondrial architecture and bioenergetics. Inhibition of the C5a/C5aR axis restored the renal mitochondrial fatty acid profile, most notably cardiolipin, and targeted metabolomics showed normalization of citric acid cycle intermediates. Proof of concept studies in human primary proximal tubule cells showed that C5aR1 signalling disrupts mitochondrial respiratory function and induces reactive oxygen species generation. Taken together, our results show that the C5a/C5aR1 axis propagates renal injury in DKD via mitochondrial reprogramming and establishes complement C5a as a new immunometabolic signalling pathway in DKD.

Methods

Patient recruitment and blood sample collection

The study was approved by the Human Research Ethics Committee at Austin Health and Alfred Health and was conducted in accordance with the principles of the Declaration of Helsinki. Participating in this study were individuals with type 1 diabetes (T1D) or type 2 diabetes (T2D) drawn from a population of patients attending the diabetes clinic at the Austin and Repatriation Medical Centre, Melbourne, Australia. As the primary referral base (80%) is from general practitioners, with only 20% referred from within the hospitals, the cohort is representative of patients with diabetes seen in the wider community. Patient recruitment methods have been described previously (12). A non-diabetic control group was also recruited from Austin Health and the Baker Heart and Diabetes Institute (Alfred Health). Written informed consent was obtained from all participants who donated blood. EDTA plasma was collected by centrifuging blood at 3500 rpm at 4°C for 15 min and storing at -80°C.

Assessment of complement components in human plasma

Commercially available ELISA kits were used to determine plasma C5a (BD OptEIA), C3a (BD OptEIA) and C5b-9 (MicroVue Quidel) according to the manufacturer's instructions.

Animal experiments

All animal experiments were performed in accordance with guidelines from the Alfred Medical Research and Education Precinct (AMREP) Animal Ethics Committee and the National Health and Medical Research Council of Australia. All rodents were housed in a temperature-controlled environment, with a 12-h light/dark cycle and access to chow (Specialty Feeds, Perth, WA, Australia) and water *ad libitum*. C57BL/6J and C5aR1$^{-/-}$ mice backcrossed onto a C57BL/6

background (gift of Prof Rick Wetsel, University of Texas (13)) were bred at AMREP Animal Services. Ins2-Akita mice (C57BL/6-*Ins2*^{Akita}/J) were purchased from the Jackson Laboratory (Bar Harbor, ME). Six week old heterozygous Ins2-Akita mice and their wildtype littermates were followed for 20 weeks. Db/db mice *(lepr(+/+)C57 BL/KsJ)* and db/h controls were purchased from the Jackson Laboratory and a colony maintained at AMREP Animal Services. Six week old db/db and db/h mice were followed for 14 weeks. Sprague-Dawley rats were sourced from AMREP Animal Services. Experimental diabetes was induced in six week old male Sprague Dawley rats (200-250g) by *i.v*. injection of streptozotocin (50mg/kg, sodium citrate buffer pH 4.5) following an overnight fast. The rat timecourse model has been previously described (14).

Diabetes was induced in 6-week-old mice by five daily intraperitoneal injections of low-dose streptozotocin (55 mg/kg; Sigma-Aldrich, St. Louis, MO). Non-diabetic group was given 0.5M sodium citrate. For the knockout study, diabetic and non-diabetic wildtype (n=7-10) and C5aR1$^{-/-}$ (n=4-12) mice were followed for 24 weeks after onset of diabetes. For the PMX53 study, diabetic and nondiabetic mice were randomized to receive either (a) the C5aR1 peptide inhibitor PMX53 (Ac-Phe-[Orn-Pro-dCha-Trp-Arg]) (synthesized as previously described (15)) at 2mg/kg body weight provided in the drinking water, or (b) drinking water alone (n=6-12), and followed for 24 weeks. At the end of the study, plasma and kidneys were collected for analysis.

Assessment of renal function and metabolic parameters

Plasma glucose was measured using a glucose colorimetric assay kit (Cayman Chemical). Glycated hemoglobin (GHb) was determined using a Cobas Integra 400 Autoanalyzer (Roche Diagnostics Corporation, USA). Urinary albumin was measured using a mouse albumin ELISA kit (Bethyl Laboratories, Montgomery, TX). Plasma cystatin C was determined using a commercially available ELISA kit from R&D Systems (MN, USA). Urinary C5a was measured

using a mouse Complement Component C5a DuoSet ELISA kit (R&D Systems). Urinary 8-isoprostane was measured using an 8-isoprostane ELISA kit (Cayman Chemical). Urine and plasma creatinine were measured using the Creatinine plus ver.2 (CREP2) on a Cobas Integra 400 plus (Roche Diagnostics). Plasma IL-18 was measure using a mouse IL-18 ELISA kit (Invitrogen, Carlsbad, Ca).

Renal histology

Kidney sections (3μm) were stained with periodic-acid Schiff (PAS) and picrosirius red. For PAS-stained sections, the degree of sclerosis in each glomerulus was subjectively graded on a scale of 0-4 with grade 0 = normal; grade 1 = sclerotic area up to 25% (minimal); grade 2 = sclerotic area 25-50% (moderate); grade 3 = sclerotic area 50-70% (moderate to severe), and grade 4 = sclerotic area 75-100% (severe). The GSI was then calculated using the following formula: GSI = (1 × n1) + (2 × n2) + (3 × n3) + (4 × n4)/n0 + n1 + n2 + n3 + n4, where nx is the number of glomeruli in each grade of glomerulosclerosis. Mesangial index was analysed from digital images of glomeruli using Image-Pro Plus v6.0 (Media Cybernetics, Bethesda, MD, USA) and expressed as percentage of PAS-stained area per glomerular cross-sectional area. For picrosirius red-stained sections, positive collagen staining (red) was examined under light microscopy (Olympus BX-50; Olympus Optical) and digitized with a high-resolution camera. All digital quantitation (Image-Pro Plus, v6.0) and assessments were performed in a blinded manner.

Immunohistochemistry

Paraffin sections of mouse kidney (4μm) were immunostained for FoxP3 (clone, FJK-16s; Affymetrix eBioscience), F4/80 (clone CI:A3-1; Abcam) or collagen IV (Southern Biotech). Briefly, endogenous peroxidases were blocked with 3% hydrogen peroxide for 15min and incubated in 0.5% skim milk/TBS for 1 hour at room temperature. Primary antibody was left on

overnight at 4°C. This was followed by incubation with biotinylated secondary antibody for 10min at room temperature. Sections were then incubated with Vectastain ABC reagent (Vector Laboratories, CA, USA). Peroxidase activity was identified by reaction with 3,3'-diaminobenzidine tetrahydrochloride (Sigma-Aldrich Pty. Ltd, NSW, Australia). Sections were counterstained with haematoxylin. All sections were examined under light microscopy (Olympus BX-50; Olympus Optical) and digitized with a high-resolution camera. All digital quantitation (Image-Pro Plus, v6.0) and assessments were performed in a blinded manner.

Quantitative real-time RT-PCR

RNA from kidney cortex and liver was extracted using TRIzol Reagent and cDNA synthesized as described previously (16). Gene expression was determined using a 7500 Fast Real-time PCR System (Applied Biosystem, VIC, Australia). Gene expression was normalized relative to 18S ribosomal RNA, and the relative fold difference in expression was calculated using the comparative $2^{-\Delta\Delta Ct}$ method.

RNA sequencing and analysis

Some 200ng of total RNA underwent ribosomal RNA depletion using the NEBNext® rRNA Depletion Kit followed by library construction using NEBNext® Ultra II™ Directional RNA Library Prep Kit for Illumina® (both from NEB, USA). Barcoded libraries underwent Illumina 100 cycle single read sequencing at AGRF, Melbourne using HiSeq v4 reagents. Reads underwent 3' trimming to remove bases with quality less than Phred 20 using Skewer (17) and were mapped with to the Ensembl mouse genome (GRCm38) using STAR (18). The resulting count matrix underwent differential analysis with the EdgeR package (19). Genes were ranked from most up-regulated to most down-regulated by multiplying the sign of the log2 fold change by the inverse of the p-value. This preranked list was used for pathway analysis using GSEA (20) with

REACTOME gene sets (21). Multi-contrast enrichment was undertaken as described previously (22).

Lipidomics

Renal cortical tissues were homogenized and sonicated in phosphate buffered saline (PBS) (pH7.4). Protein concentration was determined using the bicinchoninic acid (BCA) assay (Thermo Scientific). Lipid extraction was performed as previously described (23). Lipidomic analyses of the lipid extract were performed by liquid chromatography electrospray ionization tandem mass spectrometry modified from (24), using an AB Sciex Qtrap 4000 coupled to an Agilent 1200 HPLC. Free fatty acids were measured under the same chromatographic conditions but in negative ionization mode. Data were analyzed using Multiquant software 2.1.1 and specific lipid species were normalized to total phosphatidylcholine (PC) levels. Some lipid species were also normalized to total protein as an alternate normalization strategy.

Metabolomics

Tissue metabolites from the kidney cortex were extracted using a cryogenically cooled bead mill (25). Metabolite extracts were derivatized and analyzed by GC-MS (26). The resultant data matrix of integrated metabolite areas was log-transformed and median normalized prior to statistical analysis using MetaboAnalyst v4.0 or GraphPad Prism v7.0.

Proximal tubule cell culture and mitochondrial respiratory function

Human primary proximal tubule cells obtained from American Type Culture Collection (ATCC, USA) were maintained in Renal Epithelial Cell Basal Medium (ATCC) supplemented with the Renal Epithelial Cell Growth Kit (ATCC). PTECs, at 70-90% confluency, were seeded into 96-well XF96 cell culture microplates (Seahorse Bioscience) at 22,000 cells per well and then left to

recover for 24h in Renal Epithelial Cell Basal Medium. Cells were washed and incubated at 37ºC in DMEM containing either recombinant human C5a (500ng/ml, R&D Systems) or 500ng/ml C5a plus 2.5μM PMX53, pH 7.4 for 24 hours. The mitochondrial bioenergetic profile of primary human PTECs was assessed using the Seahorse XF96 Flux Analyzer (Seahorse Bioscience, North Billerica, MA) applying the mitochondrial stress test. Three basal oxygen consumption rate (OCR) measurements were performed and these were then repeated following sequential exposure to the ATP synthase inhibitor oligomycin (1μM), the proton ionophore carbonyl cyanide-4-(trifluoromethoxy) phenylhydrazone (FCCP, 0.75μM) and the complex III inhibitor Antimycin A (2μM) and rotenone (0.5μM). Calculation of mitochondrial respiratory function was then completed (27). At the end of the assay, cells were lysed and protein concentration was determined in each well using the BCA protein assay kit (Thermo Scientific) according to the manufacturer's instructions.

Reactive oxygen species generation

Human primary PTECs, described above, were cultured in T25 cell culture flasks ($1x10^6$ cells) and were exposed to 20nM human C5a (Complement Technology, TX, USA) or 20nM C5a plus 2.5μM PMX53 for 24 hours. After harvesting and resuspending in Hanks balanced salt solution (HBSS, with sodium bicarbonate, calcium and magnesium, 10 mM HEPES, without phenol red, pH 7.4.), cells were incubated with 10 μM 5',6'-chloromethyl-2',7'dichlorodihydro-fluorescein diacetate (CM-H_2DCFDA, Molecular Probes, Eugene, OR, USA) for 30 min at 37°C in the dark. The cells were washed twice with HBSS and analyzed on a FACS Calibur (BD, USA) flow cytometer. A minimum of 15,000 cells per sample were analyzed.

Statistical analyses

The data are expressed either as scatterplots of the data showing the mean, or as mean ± standard error of mean (SEM). Statistical analyses were performed using GraphPad Prism version 7.0 (GraphPad Software, La Jolla, CA, USA). For the clinical studies, One-way ANOVA with Tukey's post-test analysis was used to determine statistical significance. Data not normally distributed were analyzed after logarithmic transformation. For the C5aR1 knockout study, all data were analyzed by two-way ANOVA with Tukey's post hoc testing, unless otherwise stated. For the PMX53 study, all data were analyzed by one-way ANOVA with Tukey's post hoc testing, unless otherwise stated. Comparison between two groups was performed using two-tailed Student's *t*-test. If data were non-parametric, a Mann Whitney test was used. A P value <0.05 was considered statistically significant. Pearson's correlation was used to determine relationship between variables. Lipidomics data were analyzed using R (3.4.0) and all p-values were corrected for multiple comparisons using the method of Benjamini and Hochberg, controlling for the false discovery rate (FDR) (28).

Results

Both type 1 and type 2 diabetes are associated with activation of the distal pathway of complement, which is not targeted by conventional DKD trajectory modifying therapies

We explored whether the terminal complement components, including the major effector molecules C3a and C5a, and the terminal complement component C5b-9 (MAC) were altered in type 1 diabetes (T1D) and in type 2 (T2D) diabetes. Markedly elevated levels of C5a, C3a and C5b-9 were found in plasma from normoalbuminuric patients with T1D and T2D compared to non-diabetic controls (Fig. 1A-C, Table S1). These data clearly indicate that the C5aR1 axis is activated in human diabetes prior to DKD development. Since the first line therapy for patients with DKD is RAS inhibition, we determined whether this commonly used therapy could affect complement activation. The elevated level of plasma C5a, C3a and C5b-9 in patients with diabetes was not normalised in subjects treated with RAS inhibition (Fig. 1 A-C, Table S1). In patients with diabetes, there was a correlation between plasma C5a and urine albumin ($r=0.25$, $p=0.09$), however, this did not reach significance (Fig. S5A). Further, there was a negative correlation between plasma C5a and eGFR (=-0.32), however, this did not reach significance ($p=0.06$, Fig. S5B).

C5a/C5aR1 is upregulated in multiple animal models of diabetes

To investigate if complement is also activated in experimental diabetes, we evaluated the status of this axis in two disparate models, an insulin deficient model, the Ins2-Akita mouse model (a genetic model of T1D, Fig. 2A) and an insulin resistant model, the db/db mouse model (a genetic model of T2D and obesity, Fig. 2D). Indeed, *C3, C5 and C5aR1* transcripts were upregulated in the kidney in both mouse models of diabetes compared to their wildtype littermates (Fig. 2A and

D). Since the liver is the major site of complement biosynthesis, hepatic complement levels are largely reflective of systemic complement (29). Within the liver, C3 and C5aR1 transcripts were upregulated in both the Ins2-Akita and db/db mice (Fig. 2B and E). In addition, urinary excretion of C5a was markedly increased (Fig. 2C and 2F), indicating that the C5a/C5aR1 axis is upregulated in experimental diabetes and DKD, consistent with the human condition.

C5a/C5aR1 upregulation in diabetes occurs prior to the development of renal injury

To determine the timecourse of C5a activation in the development of DKD, we mapped urinary C5a excretion and renal *C5aR1* expression in a rat model of STZ-induced T1D. We have previously characterized the onset of glomerular injury in STZ-diabetic rats (14). In diabetic rats, preceding the onset of albuminuria (evident at 16 weeks (14)), at four weeks after the establishment of diabetes, there was a significant increase in *C5aR1* expression in renal cortex (Fig. 2G) and a trend toward an increase in urinary excretion of C5a, which reached significance at 16 weeks and persisted to 32 weeks (Fig. 2H). Taken together, these results suggest that upregulation of C5a/C5aR1 occurs prior to the development of detectable renal injury, consistent with complement activation playing an early key injurious role in DKD pathogenesis.

Genetic deletion of C5aR1 improves diabetes-induced renal injury

To assess the effect of genetic deletion of C5aR1 on the development of DKD, *C5aR1*$^{-/-}$ mice on a C57BL/6 background and their wildtype littermates were treated with STZ to induce diabetes. The metabolic characteristics of the mice are shown in Table 1. Plasma cystatin C was lower in wildtype diabetic mice and in *C5aR1*$^{-/-}$ diabetic mice compared to wildtype control mice (Table 1). Although there was no statistically significant difference between WT control and *C5aR1*$^{-/-}$

control mice, control *C5aR1*$^{-/-}$ mice tended to exhibit hyperfiltration. Wildtype diabetic mice had a 20-fold increase in urinary excretion of albumin compared to control mice (Fig. 3A), whilst deletion of *C5aR1* reduced by >75% diabetes-induced albuminuria (Fig. 3A). Deletion of C5aR1 also inhibited oxidative stress in the setting of diabetes as reflected by a decrease in 8-isoprostanes (Fig. 3B).

Infiltrating macrophages in the tubulointerstitium as assessed by F4/80 immunohistochemistry were increased in wildtype diabetic mice (Fig. 3C, E). Deletion of C5aR1 abrogated the increase in F4/80 positive cells in the tubulointerstitium in diabetic mice (Fig. 3C, E). Forkhead box P3 (FoxP3) regulatory T cells (or Treg) are thought to play a role in ameliorating inflammation in the diabetic kidney (30). We found a reduced number of FoxP3 positive cells in the tubulointerstitium of wildtype diabetic mice (Fig. 3D, E). C5aR1 deletion resulted in protection against FoxP3+ Treg depletion in the setting of diabetes (Fig. 3D, E).

Pharmacological inhibition of C5a/C5aR1 with PMX53 is efficacious in DKD

PMX53 is an orally active cyclic peptide antagonist of C5aR1 (6). Prior to administration to a mouse model of diabetes, we performed pharmacokinetic experiments with PMX53 in C57BL/6J mice (methods in Supplementary material). The plasma concentrations versus time profile of PMX53 via *i.v.* and *p.o.* routes demonstrated a curvilinear pattern, with a rapid clearance (Fig. S1), with the pharmacokinetic parameters reflecting a fast absorption and distribution of the drug (Table S2). An oral bioavailability of ~6% was determined as calculated by the ratio of area under the curve.

Treatment of STZ-diabetic mice with PMX53 (2mg/kg/day) in a prophylactic regimen for 24 weeks inhibited diabetes-induced albuminuria (Fig. 4A), without affecting blood glucose (Table

2). Urinary 8-isoprostanes were reduced by PMX53 treatment in diabetic mice (Fig. 4B). Renal structural injury, as reflected by both the glomerulosclerotic index (Fig. 4D, E) and mesangial matrix expansion (Fig. 4F) was significantly decreased by PMX53. Similarly, renal fibrosis was decreased with PMX53 treatment in diabetic mice (collagen IV immunostaining, Fig. 4D, G and picrosirius red staining, Fig. 4D, H).

Treatment with PMX53 was associated with a trend towards a reduction in infiltrating F4/80 positive macrophages into the tubulointerstitium in diabetic kidneys, although this was not statistically significant (Fig. 4D, I). Signaling through C5aR1 induces Th1 responses and inhibits induction of Treg (31-33). PMX53 has been shown to induce Treg activation (34). Indeed, PMX53 treatment in the diabetic setting led to an increase in FoxP3+ Tregs within the kidney (Fig. 4D, J). Furthermore, the diabetes-induced increase in the pro-inflammatory cytokine IL-18 was significantly attenuated in the plasma of diabetic mice treated with PMX53 (Fig. 4C).

Inhibition of C5aR1 restores the mitochondrial fatty acid profile and cardiolipin remodelling in DKD

We next performed transcriptomic analysis on renal cortex using RNA-Seq. The diabetes gene signature was significantly modulated by PMX53 with almost half (49%) of the genes altered by diabetes restored by PMX53 (Fig. 5A). Interestingly, REACTOME gene set analysis identified that five out of the top 10 pathways that were downregulated by PMX53 in diabetes were involved in cellular metabolism, including glycolysis, mitochondrial fatty acid beta oxidation and fatty acyl CoA biosynthesis (Fig. 5B). Of interest, the top upregulated gene by PMX53 treatment in diabetes was the Acyl-CoA dehydrogenase family, member 10 (*Acad10*, log2 fold change, FDR 1.18E-135), which was also the top downregulated gene in diabetes (log2 fold change, FDR 3.19E-132).

Acad10 is a member of the acyl-CoA dehydrogenase family of enzymes (ACADs), which participate in fatty acid oxidation (FAO) within mitochondria (35). Intriguingly, the majority of genes associated with mitochondrial fatty acid beta oxidation that were altered in diabetes were restored by PMX53 treatment (Fig. 5D and E, Table S3). Furthermore, only two out of 11 genes examined in the fatty acid metabolism pathway were significantly altered by PMX53 in the diabetic kidneys (Table S3). Validation by RT-qPCR also confirmed the *Acad10* findings (Fig. 5F). Furthermore, *Acad10* expression, which was downregulated in the renal cortex in WT diabetic mice was restored in C5aR1$^{-/-}$ diabetic mice (Fig. 5G).

The two key transcription factors responsible for the induction of lipogenic genes are sterol regulatory element binding protein (SREBP) and carbohydrate-responsive element-binding protein (ChREBP)(36; 37). To determine whether regulation of fatty acid synthesis was altered, RT-qPCR was used to determine gene expression of ChREBP and SREBP. Total ChREBP was decreased in diabetes and not altered with PMX53 (Fig. S4A) or C5aR1$^{-/-}$ (Fig. S4B). Similarly, ChREBP-α was downregulated in diabetes and not altered with PMX53 (Fig. S4C) C5aR1$^{-/-}$ (Fig. S4D). In contrast, ChREBP-β mRNA expression was highly upregulated in the kidney in the diabetic setting (~15-fold increase, Fig. S4E) and decreased in diabetic mice treated with PMX53. Interestingly, C5aR1$^{-/-}$ mice did not show a reduction in diabetes-induced ChREBP-β gene expression (Fig. S4F). There was no change in SREBP-1a (Fig. S4G&H) or SREBP-2 (Fig. S4K&L). SREBP-1c, although unchanged in the diabetic kidney from the PMX53 study cohort (Fig. S4I), was decreased in the WT diabetic kidney in the C5aR1$^{-/-}$ study cohort and mRNA expression was restored in the diabetic C5aR1$^{-/-}$ mice (Fig. S4J). Since it is thought that ChREBP-β expression best reflects total ChREBP lipogenic activity (38), these results suggest that fatty acid synthesis is increased in the diabetic kidney and normalized by PMX53.

To gain insight into the fatty acid profile of the kidney, lipidomics was undertaken. Acylcarnitines are involved in fatty acid transport into the mitochondria for oxidation and are elevated when fatty acid oxidation is supressed. Alteration in the plasma acylcarnitine profile has been observed in ~~abnormal fatty acid oxidation~~ DKD (39). However, limited studies have reported acylcarnitine levels in the kidney of T1D. Lipidomics of renal cortex showed that levels of total (Fig. S2A), short (Fig S2D) and long chain acylcarnitines (Fig. 6A, Fig S2D) were downregulated in the diabetic kidney. Total acylcarnitines were also standardized to protein (Fig. S2E) and showed the same trend as total acylcarnitines standardized to phosphatidylcholine (PC) (Fig. S2A). Inhibition of C5aR1 by PMX53 led to a restoration of total (Fig. S2A), short (Fig S2D) and long (Fig. 6A, Fig S2D) chain acylcarnitine species. Additional lipid species showed significant changes in the kidney of mice with diabetes (Fig. S2G and Table S4), including a decrease in ubiquinone (Table S4), a member of the mitochondrial electron transport chain.

Cardiolipin, which is a signature phospholipid of the inner mitochondrial membrane, is essential for optimal oxidative phosphorylation, mitochondrial architecture and mitophagy. Though the total cardiolipin content of the kidney was unchanged (Fig. S2B), we discovered striking changes to the composition of particular cardiolipin species in the diabetic kidney indicating cardiolipin remodelling (Fig. 6B and C). Lipidomics identified a decrease in nine out of 38 cardiolipin species in the diabetic kidney, notably those containing omega-3 polyunsaturated fatty acyl chains (22:6) in addition to the typical linoleyl acyl chains (18:2) (Fig. 6B). Conversely there was an increase in six out of the 38 cardiolipin species analysed (Fig. 6C), predominantly containing monounsaturated fatty acids (18:1) in addition to the linoleyl chains. This indicates loss of omega-3 polyunsaturated fatty acids from cardiolipin within the inner mitochondrial membrane and replacement with monounsaturated fatty acids at this site. PMX53 treatment restored the

composition of cardiolipin in diabetes (Fig. 6B, C), recapitulating a non-diabetic profile, suggesting that C5a may be a regulator of mitochondrial homeostasis and play a key role in metabolism.

Diabetes induces changes to mitochondrial agility which are normalised by C5aR1 inhibition

To explore the concept that the C5a/C5aR1 axis can promote changes in mitochondrial agility, targeted metabolomics was performed on renal cortex focusing on citric acid cycle metabolites. There was an increase in the citric acid cycle intermediates, cis-aconitate and isocitrate (Fig. 6D), indicating increased flux through the citric acid cycle. Lending further weight to the role of C5a/C5aR1 on metabolism, PMX53 treatment was able to restore levels of citric acid cycle intermediates to control levels.

Proof of concept studies were then performed to determine a direct effect of C5a on mitochondrial bioenergetics. Mitochondrial respiratory function was assessed in human primary proximal tubule cells (PTECs) using the Seahorse flux analyzer. Although PTECs exposed to human C5a for 24 hours did not display significantly altered basal mitochondrial oxygen consumption, C5a treatment increased mitochondrial respiration following FCCP-stimulated mitochondrial uncoupling (UCP) and ATP-linked respiration (Fig. 6E), both of which were normalized with PMX53. Finally, reactive oxygen species generation, as measured by DCFDA fluorescence, was heightened with C5a treatment and attenuated with PMX53 (Fig. 6F). These studies indicate that the C5a/C5aR1 axis can indeed promote changes in mitochondrial metabolic agility.

Discussion

The current report, including both clinical and pre-clinical studies, emphasizes a potential role for C5a in the progression of DKD and as an attractive therapeutic target for renoprotection in the setting of diabetes. Collectively, these studies show that C5a-C5aR1 signalling is involved in renal disease initiation and progression via changes in mitochondrial agility, specifically through changes in cardiolipin remodelling, mitochondrial metabolite flux and mitochondrial respiratory function.

Although the liver is the primary site of complement synthesis (40), local production of complement in the kidney, particularly within renal tubules could contribute to tissue injury in a variety of renal diseases (41). C5aR1 has been shown to be expressed on proximal tubular cells (42), podocytes (43), fibroblasts (44), mesangial cells, vascular endothelial and smooth muscle cells (11). Genome-wide transcriptome analysis showed upregulation of the complement pathway in microdissected human renal glomerular and tubule samples from patients with DKD (45). Indeed, renal cortical expression of *C5aR1* was increased early after the onset of diabetes in STZ-diabetic rats, before the development of albuminuria, and urinary excretion of C5a was evident later in diabetes, which persisted over diabetes duration. Upregulation of *C5aR1* was also found in the liver of the db/db mouse model and in the STZ mouse model, reflective also of systemic complement activation. Thus, it appears that diabetes is a state of C5a activation at both a systemic and local tissue level. A finding pertinent for translation is that plasma C5a was not reduced in patients with type 1 diabetes or type 2 diabetes treated with conventional RAS inhibitors compared to untreated diabetic individuals, indicating that the C5a-C5aR1 signalling pathway is a pathogenic pathway not effectively targeted or suppressed by conventional renoprotective therapies.

In human diabetes, plasma C5a was positively associated with urinary albumin (r=0.25), though this was a weak correlation, as it did not reach statistical significance (p=0.09). Plasma C5a was negatively correlated with eGFR (r=-0.32), however, this association did not reach significance (p=0.06). In the STZ mouse model, there was a highly significant correlation between urinary C5a and urinary albumin (r=0.80, p<0.0001). Whilst the upstream events that lead to complement activation in diabetes are unknown, complement activation in this setting is likely to be glucose-mediated. Whilst HbA_{1c} was not correlated with plasma C5a in individuals with diabetes, the increase in plasma C5a may be related to the ambient glucose concentration or to other pro-inflammatory stimuli that exist in the diabetic milieu.

Increasing evidence indicates that defective FAO contributes to renal fibrosis in chronic kidney diseases such as DKD (46; 47). In the current study, transcriptomic analyses showed that genes associated with FAO that were altered in the diabetic kidney were restored by PMX53, specifically *Acad10*. Acad10 has only been recently identified as one of the long chain acyl-CoA dehydrogenases (LCAD) (35) and its expression in the kidney is largely restricted to mitochondria (48). Intriguingly, Acad10 was ranked among the top 1% for association with early onset of T2D in a genome wide association study in Pima Indians, a population with an extremely high prevalence of renal disease in the context of diabetes (49). However, its specific association with DKD has not been reported. In the current study, inhibition of C5aR1 by PMX53, or genetic deletion of C5aR1 restored the expression of *Acad10* in the diabetic kidney, indicating that C5a-C5aR1 signalling is involved in fatty acid homeostasis by suppressing the transcription of FAO enzymes such as Acad10.

L-Carnitine (levocarnitine; 3-hydroxy-4-N-trimethylaminobutyrate) plays a pivotal role in transporting fatty acids into the mitochondria for subsequent β-oxidation. Disturbances to the relative composition of the endogenous carnitine pool which is comprised of L-carnitine with short-, medium- and long-chain acylcarnitines is associated with impaired FAO and mitochondrial dysfunction (50). Literature describing the levels of acylcarnitines in DKD has primarily focused on plasma and/or urine, and results are conflicting (39). Although a recent study has shown that circulating long chain acylcarnitines are associated with incident renal functional decline in adults (51), it is well appreciated that plasma lipid profiles may not correlate with kidney tissue levels (52). Several studies have shown changes in kidney cortical acylcarnitine levels in T2D mouse models (53; 54). However, our study is the first, to our knowledge, to determine the acylcarnitine profile in the kidney in T1D. In our mouse model of STZ-diabetes, lipidomics showed acylcarnitines to be decreased in the renal cortex. Interestingly, these findings are in contrast to findings with respect to acylcarnitine levels from T2D db/db mice where levels of acylcarnitines were found to be increased in the kidney cortex at 24 weeks of age, indicating increased FAO flux (53). This is not totally surprising, since that model is driven by insulin resistance. Several other studies have also shown that higher acylcarnitines but lower TCA intermediates in the skeletal muscle in T2D may suggest that FAO flux does not match TCA flux, leading to incomplete FAO (55). Nonetheless, very little is known of the relationship between acylcarnitine content, FAO and TCA flux in the T1D kidney. We have shown here that TCA cycle intermediates such as cis-aconitate and isocitrate are increased in the diabetic kidney, concomitant with reduced long chain acylcarnitine levels, which may suggest a dysregulation of FAO leading to a compensatory increase in these TCA metabolites. However, metabolic flux assays would be required to confirm specific changes in FAO. Most importantly, the role of C5a-C5aR1 in disturbing the mitochondrial

fatty acid signature in DKD is further substantiated by a restoration of the acylcarnitine profile and TCA intermediates in the diabetic renal cortex by PMX53. Indeed, Kang et al. (46) have shown that decreased tubule epithelial FAO induces metabolic reprogramming of tubular epithelial cells into a profibrotic phenotype. Thus, restoration of the mitochondrial fatty acid signature in the current study by inhibition of C5aR1 may be driving the attenuation of renal injury in STZ-induced diabetic mice.

Cardiolipin, the "signature" phospholipid of the inner mitochondrial membrane, is crucial for optimal mitochondrial bioenergetics and dynamics (56). The appropriate fatty acid composition of cardiolipin is crucial for maintaining normal mitochondrial structure and function, including the curvature formation of the inner mitochondrial membrane (57) and stabilization of respiratory chain complexes (58). In the current study, the kidney from mice with diabetes exhibited a markedly distinct profile of cardiolipin species, with a decrease in species containing omega-3 (22:6) fatty acids and an incorporation of species containing monounsaturated (oleic acid) fatty acids. Cardiolipin is highly sensitive to oxidative damage induced by reactive oxygen species, due to its high content of polyunsaturated fatty acids (59). Indeed, we found evidence of increased oxidative stress with increased lipid peroxidation (8-isoprostanes) in the diabetic kidney which may have precipitated cardiolipin remodelling. In the current study, inhibition of C5aR1 reversed the aberrant cardiolipin profile in the diabetic renal cortex, indicating that targeting the C5a-C5aR1 axis could prevent detrimental cardiolipin remodelling and restore mitochondrial homeostasis in DKD. A recent study implicated a role for C5a-C5aR1 signalling in the regulation of lipid metabolism in diabetes, by using an aptamer to C5aR1 in a model of T2D (db/db mouse), which showed a reduction in serum triglycerides and a decrease in the expression of genes involved in

the regulation of fatty acid synthesis such as DGAT1 and SREBP-1 (60). The current study is the first to demonstrate that the C5a-C5aR1 axis may be ~~is~~ involved in mitochondrial cardiolipin remodeling, potentially resulting in a mitochondrial defect.

Results from our studies have important clinical implications. The upstream positioning of complement in inflammatory propagation renders it an attractive system for targeted modulation (61). A suite of complement inhibitors have been developed which target complement at various stages of the activation pathway including at the level of C3 (e.g., Compstatin), C5 (e.g., Eculizumab) and C5aR1 (e.g., PMX53 and Avacopan) (61). However, selective targeting of C5a/C5aR1 is considered to be more amenable for chronic disease management since the immune defence functions of the proximal complement system, such as opsonization and formation of membrane attack complex, are preserved, while the properties of C5a that promote inflammation and metabolic reprogramming are impeded. PMX53, an orally active peptide antagonist of C5a (6), is one of the most widely studied and utilized inhibitors of C5aR1 in models of inflammatory diseases, albeit not previously in diabetes. Although PMX53 was determined to have rapid clearance/distribution and low oral bioavailability following administration to mice, it is a non-competitive and effectively irreversible antagonist with extended pharmacodynamics following oral treatment (62). In the clinical context, early phase Ib/IIa trials for the treatment of rheumatoid arthritis have found PMX53 to be safe and well tolerated when administered orally (63). With the potential to advance into clinical development, this is the first study to use an orally bioavailable agent, PMX53, in the DKD setting.

We note that there are limitations to this study: 1) RNA-Seq and lipidomics were performed on renal cortical tissue, so we cannot determine which cell types are most affected by diabetes and/or C5aR1 inhibition; 2) the role of an alternate anaphylatoxin of the complement system, C3a, which was also increased in the plasma of patients with diabetes, was not examined. However, dual function of C3a and its receptor C3aR, in the control of inflammation (64), as well as a lack of specific antagonists in clinical development (65) are major impediments to the translational potential of C3a; and finally 3) stable isotope flux analysis to assess fatty acid oxidation could not be performed.

In summary, this series of clinical, preclinical and in vivo mechanistic studies indicate that the C5a-C5aR1 signalling axis: (i) plays a crucial role in the pathogenesis of DKD via mitochondrial reprogramming, (ii) is not yet touched by conventional clinical therapies of DKD, (iii) may be directly targeted to in order to potentiate meaningful renoprotection in diabetes. Targeting the C5a-C5aR1 pathway with orally bioavailable antagonists, such as PMX53, could potentially fulfil the unmet clinical need of treating and preventing the development of DKD, the major cause of end stage renal disease worldwide.

Acknowledgments: We thank the following people for their technical assistance: Maryann Arnstein, Sally. A. Penfold, Brooke E. Harcourt, Gavin. C. Higgins, Runa. S. Lindblom, Karly. C. Sourris, Natalie Mellet and Carlos Rosado. We acknowledge the use of Illumina sequencing at AGRF (and the support it receives from the Commonwealth of Australia). We thank Antony Kaspi for bioinformatics support related to multidimensional pathway analysis and acknowledge the Baker IDI Biobank Melbourne, Australia for providing human plasma samples. The authors also acknowledge use of the facilities of Monash Histology Platform and Metabolomics Australia, Bio21.

Author contributions: SMT researched the data, performed the experiments and wrote the manuscript. MZ and AEO performed the RNA-Seq and bioinformatics and assisted with writing the manuscript. VTB , MS, AL and TVN performed laboratory experiments. RL, STB, GJ, AS, DAP, RJM provided clinical samples. EIE oversaw the clinical studies and drafted the paper. RAW provided the C5aR1$^{-/-}$ mice. PJM and KH performed the lipidomics. SW, JMF, MEC and DCH provided input into drafting the manuscript. VK generated PMX53 and performed pharmacokinetics. TMW assisted with experimental design and provided intellectual input into the study. MTC conceived, designed and oversaw the studies and wrote the manuscript.

Guarantor Statement: MTC is the guarantor of this work and, as such, had full access to all the data in the study and takes responsibility for the integrity of the data and the accuracy of the data analysis.

Conflict of Interest: None.

Funding: This study was supported by a JDRF Innovative Grant (1-SRA-2014-261-Q-R) and a Diabetes Australia Research Program grant. SMT is supported by a JDRF Advanced Postdoctoral Fellowship. EIE was supported by a Viertel Clinical Investigatorship, RACP – JDRF Fellowship

and Sir Edward Weary Dunlop Medical Research Foundation and Diabetes Australia Research Program research grants. TMW was supported by an Australian National Health and Medical Research Council Career Development Fellowship (APP1105420). MTC is the recipient of a Career Development Award from JDRF Australia, the recipient of the Australian Research Council Special Research Initiative in Type 1 Juvenile Diabetes.

Data and Resource Availability: Sequence data has been deposited to NCBI Gene Expression Omnibus under accession number GSE118089.

References

1. Thomas MC, Weekes AJ, Broadley OJ, Cooper ME, Mathew TH: The burden of chronic kidney disease in Australian patients with type 2 diabetes (the NEFRON study). Med J Aust 2006;185:140-144
2. Nathan DM, Zinman B, Cleary PA, Backlund J-YC, Genuth S, Miller R, Orchard TJ, Diabetes C, Complications Trial/Epidemiology of Diabetes I, Complications Research G: Modern-Day Clinical Course of Type 1 Diabetes Mellitus After 30 Years' Duration: The Diabetes Control and Complications Trial/Epidemiology of Diabetes Interventions and Complications and Pittsburgh Epidemiology of Diabetes Complications Experience (1983-2005). Archives of internal medicine 2009;169:1307-1316
3. Tesch GH: Diabetic nephropathy – is this an immune disorder? Clinical Science 2017;131:2183-2199
4. Walport MJ: Complement. New England Journal of Medicine 2001;344:1058-1066
5. Flyvbjerg A: The role of the complement system in diabetic nephropathy. Nature Reviews Nephrology 2017;13:311-318
6. Woodruff TM, Nandakumar KS, Tedesco F: Inhibiting the C5–C5a receptor axis. Molecular Immunology 2011;48:1631-1642
7. Liu L, Zhang Y, Duan X, Peng Q, Liu Q, Zhou Y, Quan S, Xing G: C3a, C5a Renal Expression and Their Receptors are Correlated to Severity of IgA Nephropathy. J Clin Immunol 2014;34:224-232
8. Peng Q, Li K, Smyth LA, Xing G, Wang N, Meader L, Lu B, Sacks SH, Zhou W: C3a and C5a Promote Renal Ischemia-Reperfusion Injury. Journal of the American Society of Nephrology 2012;23:1474-1485
9. Williams AL, Gullipalli D, Ueda Y, Sato S, Zhou L, Miwa T, Tung KS, Song W-C: C5 inhibition prevents renal failure in a mouse model of lethal C3 glomerulopathy. Kidney International 2017;91:1386-1397
10. Bao L, Osawe I, Puri T, Lambris JD, Haas M, Quigg RJ: C5a promotes development of experimental lupus nephritis which can be blocked with a specific receptor antagonist. European Journal of Immunology 2005;35:2496-2506
11. Abe K, Miyazaki M, Koji T, Furusu A, Nakamura-Kurashige T, Nishino T, Ozono Y, Harada T, Sakai H, Kohno S: Enhanced expression of complement C5a receptor mRNA in human diseased kidney assessed by in situ hybridization. Kidney Int 2001;60:137-146
12. Libianto R, Jerums G, Lam Q, Chen A, Baqar S, Pyrlis F, Macisaac RJ, Moran J, Ekinci EI: Relationship between urinary sodium excretion and serum aldosterone in patients with diabetes in the presence and absence of modifiers of the renin-angiotensin-aldosterone system. Clin Sci (Lond) 2014;126:147-154
13. Hollmann TJ, Mueller-Ortiz SL, Braun MC, Wetsel RA: Disruption of the C5a receptor gene increases resistance to acute Gram-negative bacteremia and endotoxic shock: opposing roles of C3a and C5a. Mol Immunol 2008;45:1907-1915
14. Coughlan MT, Nguyen TV, Penfold SA, Higgins GC, Thallas-Bonke V, Tan SM, Van Bergen NJ, Sourris KC, Harcourt BE, Thorburn DR, Trounce IA, Cooper ME, Forbes JM: Mapping time-course mitochondrial adaptations in the kidney in experimental diabetes. Clin Sci (Lond) 2016;130:711-720
15. March DR, Proctor LM, Stoermer MJ, Sbaglia R, Abbenante G, Reid RC, Woodruff TM, Wadi K, Paczkowski N, Tyndall JD, Taylor SM, Fairlie DP: Potent cyclic antagonists of the

complement C5a receptor on human polymorphonuclear leukocytes. Relationships between structures and activity. Mol Pharmacol 2004;65:868-879
16. Tan SM, Sharma A, Yuen DYC, Stefanovic N, Krippner G, Mugesh G, Chai Z, de Haan JB: The Modified Selenenyl Amide, M-hydroxy Ebselen, Attenuates Diabetic Nephropathy and Diabetes-Associated Atherosclerosis in ApoE/GPx1 Double Knockout Mice. PLoS ONE 2013;8:e69193
17. Jiang H, Lei R, Ding S-W, Zhu S: Skewer: a fast and accurate adapter trimmer for next-generation sequencing paired-end reads. BMC Bioinformatics 2014;15:182
18. Dobin A, Davis CA, Schlesinger F, Drenkow J, Zaleski C, Jha S, Batut P, Chaisson M, Gingeras TR: STAR: ultrafast universal RNA-seq aligner. Bioinformatics 2013;29:15-21
19. Robinson MD, McCarthy DJ, Smyth GK: edgeR: a Bioconductor package for differential expression analysis of digital gene expression data. Bioinformatics 2010;26:139-140
20. Subramanian A, Kuehn H, Gould J, Tamayo P, Mesirov JP: GSEA-P: a desktop application for Gene Set Enrichment Analysis. Bioinformatics 2007;23:3251-3253
21. Fabregat A, Sidiropoulos K, Garapati P, Gillespie M, Hausmann K, Haw R, Jassal B, Jupe S, Korninger F, McKay S, Matthews L, May B, Milacic M, Rothfels K, Shamovsky V, Webber M, Weiser J, Williams M, Wu G, Stein L, Hermjakob H, D'Eustachio P: The Reactome pathway Knowledgebase. Nucleic Acids Research 2016;44:D481-D487
22. Quaife-Ryan GA, Sim CB, Ziemann M, Kaspi A, Rafehi H, Ramialison M, El-Osta A, Hudson JE, Porrello ER: Multicellular Transcriptional Analysis of Mammalian Heart Regeneration. Circulation 2017;136:1123-1139
23. Tham YK, Huynh K, Mellett NA, Henstridge DC, Kiriazis H, Ooi JYY, Matsumoto A, Patterson NL, Sadoshima J, Meikle PJ, McMullen JR: Distinct lipidomic profiles in models of physiological and pathological cardiac remodeling, and potential therapeutic strategies. Biochimica et biophysica acta 2018;1863:219-234
24. Huynh K, Barlow CK, Jayawardana KS, Weir JM, Mellett NA, Cinel M, Magliano DJ, Shaw JE, Drew BG, Meikle PJ: High-Throughput Plasma Lipidomics: Detailed Mapping of the Associations with Cardiometabolic Risk Factors. Cell Chem Biol 2019;26:71-84 e74
25. Kowalski GM, De Souza DP, Burch ML, Hamley S, Kloehn J, Selathurai A, Tull D, O'Callaghan S, McConville MJ, Bruce CR: Application of dynamic metabolomics to examine in vivo skeletal muscle glucose metabolism in the chronically high-fat fed mouse. Biochemical and biophysical research communications 2015;462:27-32
26. Overgaard AJ, Weir JM, De Souza DP, Tull D, Haase C, Meikle PJ, Pociot F: Lipidomic and metabolomic characterization of a genetically modified mouse model of the early stages of human type 1 diabetes pathogenesis. Metabolomics : Official journal of the Metabolomic Society 2016;12:13
27. McGee SL, Sadli N, Morrison S, Swinton C, Suphioglu C: DHA protects against zinc mediated alterations in neuronal cellular bioenergetics. Cell Physiol Biochem 2011;28:157-162
28. Benjamini Y, Hochberg Y: Controlling the False Discovery Rate - a Practical and Powerful Approach to Multiple Testing. J R Stat Soc B 1995;57:289-300
29. Qin X, Gao B: The complement system in liver diseases. Cell Mol Immunol 2006;3:333-340
30. Lim AKH, Tesch GH: Inflammation in Diabetic Nephropathy. Mediators of Inflammation 2012;2012:12
31. Strainic MG, Shevach EM, An F, Lin F, Medof ME: Absence of signaling into CD4(+) cells via C3aR and C5aR enables autoinductive TGF-beta1 signaling and induction of Foxp3(+) regulatory T cells. Nat Immunol 2013;14:162-171

32. Weaver DJ, Jr., Reis ES, Pandey MK, Kohl G, Harris N, Gerard C, Kohl J: C5a receptor-deficient dendritic cells promote induction of Treg and Th17 cells. Eur J Immunol 2010;40:710-721
33. van der Touw W, Cravedi P, Kwan W-h, Paz-Artal E, Merad M, Heeger PS: Cutting Edge: Receptors for C3a and C5a Modulate Stability of Alloantigen-Reactive Induced Regulatory T Cells. The Journal of Immunology 2013;190:5921-5925
34. Dick J, Gan PY, Ford SL, Odobasic D, Alikhan MA, Loosen SH, Hall P, Westhorpe CL, Li A, Ooi JD, Woodruff TM, Mackay CR, Kitching AR, Hickey MJ, Holdsworth SR: C5a receptor 1 promotes autoimmunity, neutrophil dysfunction and injury in experimental anti-myeloperoxidase glomerulonephritis. Kidney Int 2017;
35. He M, Pei Z, Mohsen A-W, Watkins P, Murdoch G, Van Veldhoven PP, Ensenauer R, Vockley J: Identification and Characterization of New Long Chain Acyl-CoA Dehydrogenases. Molecular genetics and metabolism 2011;102:418-429
36. Abdul-Wahed A, Guilmeau S, Postic C: Sweet Sixteenth for ChREBP: Established Roles and Future Goals. Cell Metab 2017;26:324-341
37. Wang Y, Viscarra J, Kim SJ, Sul HS: Transcriptional regulation of hepatic lipogenesis. Nat Rev Mol Cell Biol 2015;16:678-689
38. Herman MA, Peroni OD, Villoria J, Schon MR, Abumrad NA, Bluher M, Klein S, Kahn BB: A novel ChREBP isoform in adipose tissue regulates systemic glucose metabolism. Nature 2012;484:333-338
39. Chuang W-H, Arundhathi A, Lu C, Chen C-C, Wu W-C, Susanto H, Purnomo JDT, Wang C-H: Altered plasma acylcarnitine and amino acid profiles in type 2 diabetic kidney disease. Metabolomics : Official journal of the Metabolomic Society 2016;12:108
40. Morgan BP, Gasque P: Extrahepatic complement biosynthesis: where, when and why? Clinical & Experimental Immunology 1997;107:1-7
41. Zhou W, Marsh JE, Sacks SH: Intrarenal synthesis of complement. Kidney Int 2001;59:1227-1235
42. Zahedi R, Braun M, Wetsel RA, Ault BH, Khan A, Welch TR, Frenzke M, Davis AE: The C5a receptor is expressed by human renal proximal tubular epithelial cells. Clinical & Experimental Immunology 2000;121:226-233
43. Weiss S, Rosendahl A, Czesla D, Meyer-Schwesinger C, Stahl RAK, Ehmke H, Kurts C, Zipfel PF, Köhl J, Wenzel UO: The complement receptor C5aR1 contributes to renal damage but protects the heart in angiotensin II-induced hypertension. American Journal of Physiology - Renal Physiology 2016;310:F1356-F1365
44. Mathern DR, Heeger PS: Molecules Great and Small: The Complement System. Clinical journal of the American Society of Nephrology : CJASN 2015;10:1636-1650
45. Woroniecka KI, Park AS, Mohtat D, Thomas DB, Pullman JM, Susztak K: Transcriptome analysis of human diabetic kidney disease. Diabetes 2011;60:2354-2369
46. Kang HM, Ahn SH, Choi P, Ko Y-A, Han SH, Chinga F, Park ASD, Tao J, Sharma K, Pullman J, Bottinger EP, Goldberg IJ, Susztak K: Defective fatty acid oxidation in renal tubular epithelial cells plays a key role in kidney fibrosis development. Nature medicine 2015;21:37-46
47. Herman-Edelstein M, Scherzer P, Tobar A, Levi M, Gafter U: Altered renal lipid metabolism and renal lipid accumulation in human diabetic nephropathy. Journal of Lipid Research 2014;55:561-572
48. Bloom K, Mohsen A-W, Karunanidhi A, El Demellawy D, Reyes-Múgica M, Wang Y, Ghaloul-Gonzalez L, Otsubo C, Tobita K, Muzumdar R, Gong Z, Tas E, Basu S, Chen J, Bennett

M, Hoppel C, Vockley J: Investigating the link of ACAD10 deficiency to type 2 diabetes mellitus. Journal of Inherited Metabolic Disease 2018;41:49-57
49. Bian L, Hanson RL, Muller YL, Ma L, Investigators M, Kobes S, Knowler WC, Bogardus C, Baier LJ: Variants in ACADIO are associated with type 2 diabetes, insulin resistance and lipid oxidation in Pima Indians. Diabetologia 2010;53:1349-1353
50. Reuter SE, Evans AM: Carnitine and Acylcarnitines. Clinical Pharmacokinetics 2012;51:553-572
51. Wang F, Sun L, Sun Q, Liang L, Gao X, Li R, Pan A, Li H, Deng Y, Hu FB, Wu J, Zeng R, Lin X: Associations of Plasma Amino Acid and Acylcarnitine Profiles with Incident Reduced Glomerular Filtration Rate. Clinical journal of the American Society of Nephrology : CJASN 2018;13:560-568
52. Sas KM, Lin JH, Rajendiran TM, Soni T, Nair V, Hinder LM, Jagadish HV, Gardner TW, Abcouwer SF, Brosius FC, Feldman EL, Kretzler M, Michailidis G, Pennathur S: Shared and distinct lipid-lipid interactions in plasma and affected tissues in a diabetic mouse model. Journal of Lipid Research 2018;59:173-183
53. Sas KM, Kayampilly P, Byun J, Nair V, Hinder LM, Hur J, Zhang H, Lin C, Qi NR, Michailidis G, Groop PH, Nelson RG, Darshi M, Sharma K, Schelling JR, Sedor JR, Pop-Busui R, Weinberg JM, Soleimanpour SA, Abcouwer SF, Gardner TW, Burant CF, Feldman EL, Kretzler M, Brosius FC, 3rd, Pennathur S: Tissue-specific metabolic reprogramming drives nutrient flux in diabetic complications. JCI insight 2016;1:e86976
54. Weiser A, Giesbertz P, Daniel H, Spanier B: Acylcarnitine Profiles in Plasma and Tissues of Hyperglycemic NZO Mice Correlate with Metabolite Changes of Human Diabetes. Journal of Diabetes Research 2018;2018:9
55. Schooneman MG, Vaz FM, Houten SM, Soeters MR: Acylcarnitines: reflecting or inflicting insulin resistance? Diabetes 2013;62:1-8
56. Claypool SM, Koehler CM: The complexity of cardiolipin in health and disease. Trends Biochem Sci 2012;37:32-41
57. Renner LD, Weibel DB: Cardiolipin microdomains localize to negatively curved regions of Escherichia coli membranes. Proc Natl Acad Sci U S A 2011;108:6264-6269
58. Claypool SM, Oktay Y, Boontheung P, Loo JA, Koehler CM: Cardiolipin defines the interactome of the major ADP/ATP carrier protein of the mitochondrial inner membrane. J Cell Biol 2008;182:937-950
59. Toda N, Imamura T, Okamura T: Alteration of nitric oxide-mediated blood flow regulation in diabetes mellitus. Pharmacology & Therapeutics 2010;127:189-209
60. Yiu WH, Li RX, Wong DWL, Wu HJ, Chan KW, Chan LYY, Leung JCK, Lai KN, Sacks SH, Zhou W, Tang SCW: Complement C5a inhibition moderates lipid metabolism and reduces tubulointerstitial fibrosis in diabetic nephropathy. Nephrology, dialysis, transplantation : official publication of the European Dialysis and Transplant Association - European Renal Association 2017;
61. Ricklin D, Lambris JD: Progress and trends in complement therapeutics. Advances in experimental medicine and biology 2013;735:1-22
62. Seow V, Lim J, Cotterell AJ, Yau MK, Xu W, Lohman RJ, Kok WM, Stoermer MJ, Sweet MJ, Reid RC, Suen JY, Fairlie DP: Receptor residence time trumps drug-likeness and oral bioavailability in determining efficacy of complement C5a antagonists. Sci Rep 2016;6:24575

63. Vergunst CE, Gerlag DM, Dinant H, Schulz L, Vinkenoog M, Smeets TJ, Sanders ME, Reedquist KA, Tak PP: Blocking the receptor for C5a in patients with rheumatoid arthritis does not reduce synovial inflammation. Rheumatology (Oxford) 2007;46:1773-1778
64. Coulthard LG, Woodruff TM: Is the Complement Activation Product C3a a Proinflammatory Molecule? Re-evaluating the Evidence and the Myth. The Journal of Immunology 2015;194:3542-3548
65. Hawksworth OA, Li XX, Coulthard LG, Wolvetang EJ, Woodruff TM: New concepts on the therapeutic control of complement anaphylatoxin receptors. Molecular Immunology 2017;89:36-43

Tables

Table 1: Basic characteristics of wildtype nondiabetic control, wildtype diabetic, C5aR1 knockout ($^{-/-}$) nondiabetic control and C5aR1$^{-/-}$ diabetic mice after 24 weeks of diabetes.

	WT Con	WT Diab	C5aR1$^{-/-}$ Con	C5aR1$^{-/-}$ Diab
BW, g	33.5±0.7	23.1±1.3****	38.0±1.3*	23.3±0.8††††
Plasma glucose, mg/dL	284±19	629±56**	329±27	578±73**
HbA_{1c}, % (mmol/mol)	4.3±0.04 (23±1)	13.3±0.3**** (120±3)	4.4±0.2 (21±1)	13.2±0.6†††† (120±7)
CrCl, ml/min/m^2	18.9±2.5	30.6±7.8	27.0±8.6	26.3±3.4
Cystatin C, ng/ml	450.3±23.4	284.9±31.3***	374.8±24.1	306.0±25.5**
L.Kid:BW, mg/g	4.8±0.2	11.6±0.8****	5.1±0.3	10.8±.6††††

*P<0.05, **P<0.01, ***P<0.001, ****P<0.0001 vs WT Con; ††P<0.01, †††P<0.001, ††††P<0.0001 vs C5aR1$^{-/-}$ Con. Data are presented as mean±SEM.

BW = body weight; HbA1c = haemoglobin A1c; CrCl = creatinine clearance; L.Kid = left kidney; WT = wildtype; Con = control; Diab = diabetic.

Table 2: Basic characteristics of nondiabetic control and STZ diabetic mice treated with vehicle or C5aR1 antagonist, PMX53 for 24 weeks.

	Con	Con+PMX53	Diab	Diab+PMX53
BW, g	34±1	35±1	23±1****	29±1*###
Plasma glucose, mg/dL	258±27	201±20	639±38****	559±80***
HbA1c, % (mmol/mol)	5.0±0.2 (31±4)	5.4±0.1 (36±4)	12.2±1.4** (123±3)	9.4 ±1.1 (79±12)
CrCl, ml/min/m²	17.7±4.5	15.7±1.8	28.4±5.2	28.7±3.4
Cystatin C, ng/ml	464.8±25.8	467.8±49.5	287.5±25.6**	373.4±32.2
L.Kid:BW, mg/g	5.368±0.218	5.355±0.190	10.67±0.541****	7.923±0.245**###

****P<0.0001, ***P<0.001, **P<0.01, *P<0.05 vs Con; ###P<0.001, #P<0.05 vs Diab.

BW = body weight; HbA1c = haemoglobin A1c; CrCl = creatinine clearance; L.Kid = left kidney; WT = wildtype; Con = control; Diab = diabetic.

Figure legends

Fig. 1. **Complement activation in patients with type 1 diabetes and type 2 diabetes is not targeted by classical clinical therapy.** Plasma C5a (**A**), C3a (**B**) and C5b-9 (**C**) were measured in non-diabetic control individuals (Con, n=38), in patients with type 1 diabetes (T1D, n=18) or type 2 diabetes (T2D, n=20), and in patients with diabetes treated with renin-angiotensin system (RAS) inhibitors (T1D+RAS, n=19; T2+RAS, n=20). The line within the scatterplot represents the mean. Comparison between the groups was performed using one-way ANOVA followed by Tukey's test. ***P<0.001 vs Con.

Fig. 2. The C5a/C5aR1 axis is upregulated in diverse mouse models of diabetes. (**A**) Renal cortical and (**B**) liver *C3, C5 and C5aR1* expression in the Ins2-Akita mouse model (n=8-20 mice per group, *P<0.05, **P<0.01, ***P<0.001, ****P<0.0001 vs WT). (**C**) Urinary excretion of C5a in Ins2-Akita mice (n=8-13 mice per group, **P<0.01 vs WT). (**D**) Renal cortical and (**E**) liver *C3, C5 and C5aR1* expression in the db/db mouse model (n=3-9 mice per group, *P<0.05, **P<0.01, ***P<0.001 vs db/h). (**F**) Urinary excretion of C5a in db/db mice (n=9-18 mice per group, ***P<0.001 vs db/h). STZ-diabetic rats were followed for 4, 8, 16 and 32 weeks and *C5aR1* mRNA expression was determined (**G**) and urinary C5a excretion (**H**), n=6-10 rats per group. *P<0.05, **P<0.01 vs Con at the same timepoint. The line within the scatterplot represents the mean.

Fig. 3. Genetic deletion of C5aR1 protects against diabetes-induced inflammation and renal injury. Urinary albumin (**A**) and 8-isoprostane (**B**) were determined in wildtype control and diabetic mice and in C5aR1$^{-/-}$ control and diabetic mice. (**C**) F4/80+ cells in the renal cortex (C, E

top row). (**D**) FoxP3+ cells the renal cortex (D, E bottom row). Original magnification ×200. Scale bar = 50μm. n = 4-12 mice/group. *P<0.05, **P<0.01, ****P<0.0001 vs WT Con; #P<0.05, ##P<0.01, ###P<0.001 vs WT Diab; ^^^P<0.001 vs C5aR1$^{-/-}$ Con. The line within the scatterplot represents the mean.

Fig. 4. C5aR1 inhibition by PMX53 is efficacious in DKD. Wildtype control and STZ-diabetic mice were treated with 2mg/kg/day PMX53 for 24 weeks and urinary albumin (**A**) 8-isoprostane (**B**) and plasma IL-18 (**C**) were determined. Renal histology was examined by staining paraffin-embedded sections with Periodic acid-Schiff (PAS) and glomerulosclerotic index (**D, E**) and mesangial matrix expansion (**D, F**) was quantitated. Glomerular Collagen IV deposition was determined (**D, G**). Kidney fibrotic area was determined by picrorsirius red staining **(D, H)**. Inflammatory F4/80+ cells **(D, I)** and anti-inflammatory FoxP3+ cells **(D, J)** in the kidney were examined by immunohistochemistry. Original magnification ×400 and scale bar = 25μm for PAS and Col IV. Original magnification ×200 and scale bar = 50μm for picrosirius red, F4/80 and FoxP3. n = 6-12 mice/group. *P<0.05, ***P<0.001, ****P<0.0001 vs Con; #P<0.05, ##P<0.01, ####P<0.0001 vs Diab. The line within the scatterplot represents the mean.

Fig. 5. RNA-Seq analysis reveals a role for C5aR1 in pathways involved in mitochondrial fatty acid beta-oxidation. (**A**) Rank-rank density plot of differential gene expression due to diabetes and PMX53 treatment. (**B**) GSEA analysis of diabetes vs diabetes+PMX53 showing the top REACTOME pathways, with mitochondrial fatty acid beta-oxidation pathway highlighted red. (**C**) MA plot of top differential genes in diabetes vs diabetes+PMX53 groups with the top three downregulated and top three upregulated genes highlighted. (**D**) Rank-rank density plot of

differential genes in the mitochondrial fatty acid beta-oxidation pathway. (**E**) Gene set enrichment analysis highlighted genes that were altered by PMX53 in the mitochondrial fatty acid beta-oxidation pathway in diabetic mice. (**F**) *Acad10* expression in PMX53 treated mice and (**G**) C5aR1$^{-/-}$ mice. mice/group. n = 6-12, **P<0.01 vs Con or WT Con, $^{\#\#}$P<0.01 vs Diab or WT Diab. The line within the scatterplot represents the mean.

Fig. 6. Diabetes induces changes to mitochondrial agility including kidney cardiolipin remodelling and enhanced TCA cycle intermediate generation, which are normalised by C5aR1 inhibition. Lipidomics of renal cortex was performed to determine (**A**) Acylcarnitine species and (**B**) Cardiolipin species that were downregulated in diabetes and restored by PMX53 treatment, or (**C**) Cardiolipin species that were upregulated in diabetes and attenuated by PMX53 treatment. Data are mean±SEM, n=6-12 mice/group. (**D**) TCA cycle intermediates in renal cortex were determined by metabolomics, n=6-12 mice/group. *P<0.05, ***P<0.001 vs Con, $^{\#}$P<0.05, $^{\#\#}$P<0.01, $^{\#\#\#}$P<0.001 vs Diab. (**E**) Human primary proximal tubule epithelial cells (PTECs) were exposed to C5a or C5a plus PMX53 for 24 hours and mitochondrial oxygen consumption rate (OCR), including basal, carbonyl cyanide-4-(trifluoromethoxy) phenylhydrazone (FCCP)-uncoupled (UCR), and ATP-linked respiration was determined by Seahorse Flux Analyzer. Values are mean±SEM, n≥9 replicates per group. *P<0.05 vs Con, $^{\#}$P<0.05 vs C5a-treated cells. (**F**) PTECs were exposed to C5a or C5a plus PMX53 for 24 hours and reactive oxygen species production was determined using the DCFDA probe with flow cytometry detection. Values are mean±SEM, n=3 replicates per group. *P<0.05 vs Con, $^{\#}$P<0.05 vs C5a-treated cells.

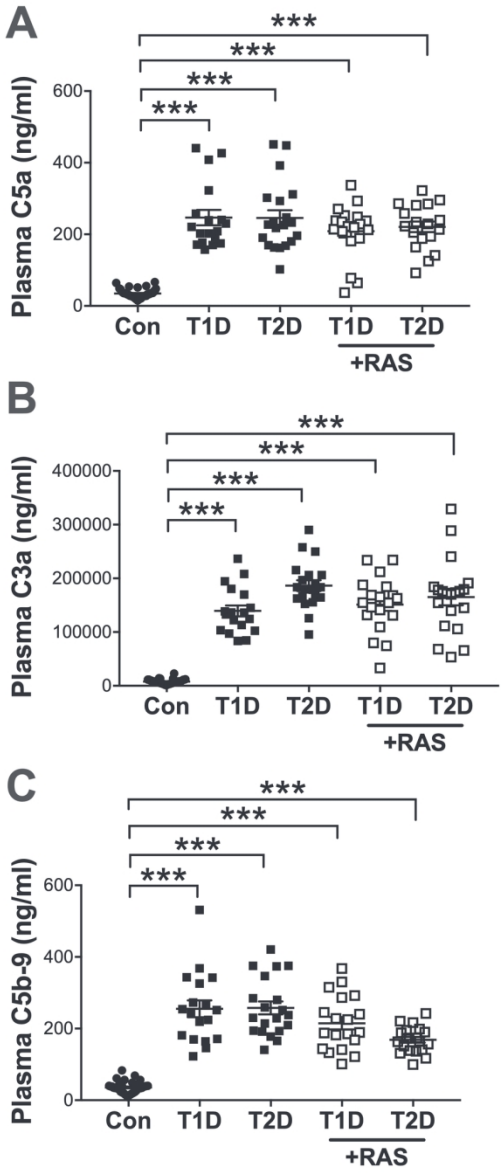

Figure 1. Complement activation in patients with type 1 diabetes and type 2 diabetes is not targeted by classical clinical therapy. Plasma C5a (A), C3a (B) and C5b-9 (C) were measured in non-diabetic control individuals (Con, n=38), in patients with type 1 diabetes (T1D, n=18) or type 2 diabetes (T2D, n=20), and in patients with diabetes treated with renin-angiotensin system (RAS) inhibitors (T1D+RAS, n=19; T2+RAS, n=20). The line within the scatterplot represents the mean. Comparison between the groups was performed using one-way ANOVA followed by Tukey's test. ***P<0.001 vs Con.

92x191mm (300 x 300 DPI)

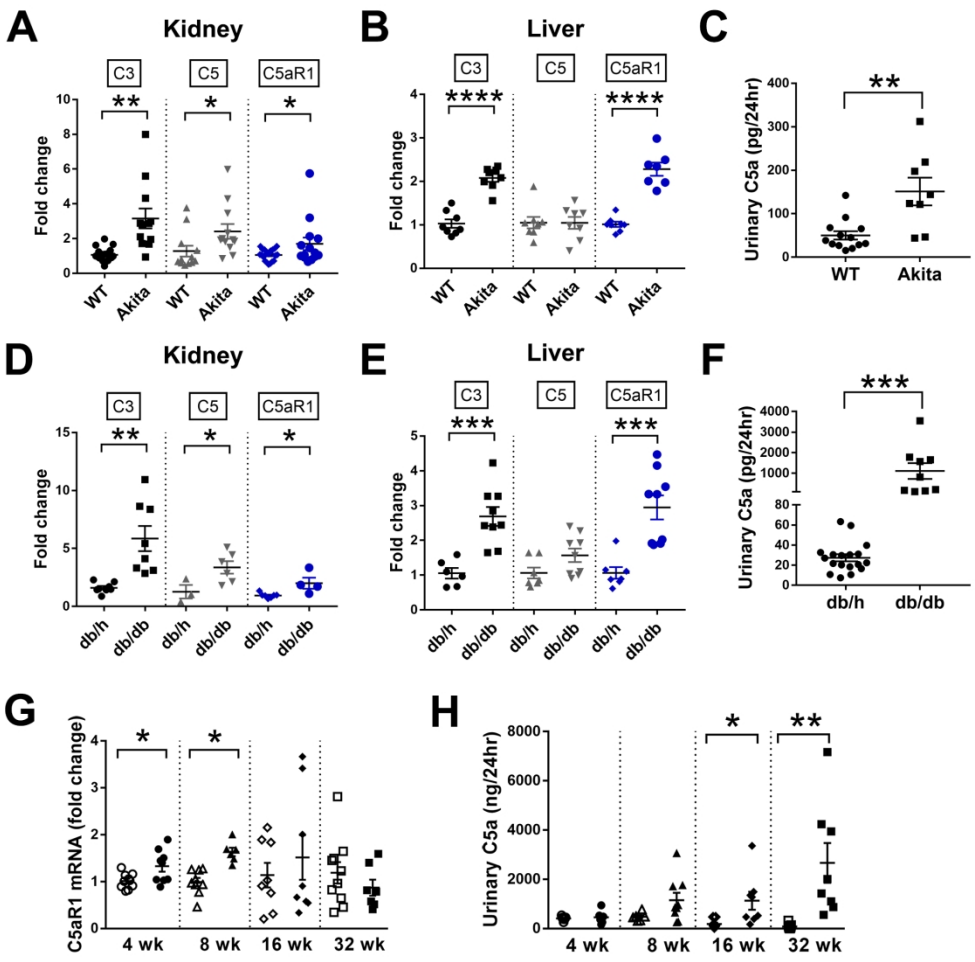

Figure 2. The C5a/C5aR1 axis is upregulated in diverse mouse models of diabetes. (A) Renal cortical and (B) liver C3, C5 and C5aR1 expression in the Ins2-Akita mouse model (n=8-20 mice per group, *P<0.05, **P<0.01, ***P<0.001, ****P<0.0001 vs WT). (C) Urinary excretion of C5a in Ins2-Akita mice (n=8-13 mice per group, **P<0.01 vs WT). (D) Renal cortical and (E) liver C3, C5 and C5aR1 expression in the db/db mouse model (n=3-9 mice per group, *P<0.05, **P<0.01, ***P<0.001 vs db/h). (F) Urinary excretion of C5a in db/db mice (n=9-18 mice per group, ***P<0.001 vs db/h). STZ-diabetic rats were followed for 4, 8, 16 and 32 weeks and C5aR1 mRNA expression was determined (G) and urinary C5a excretion (H), n=6-10 rats per group. *P<0.05, **P<0.01 vs Con at the same timepoint. The line within the scatterplot represents the mean.

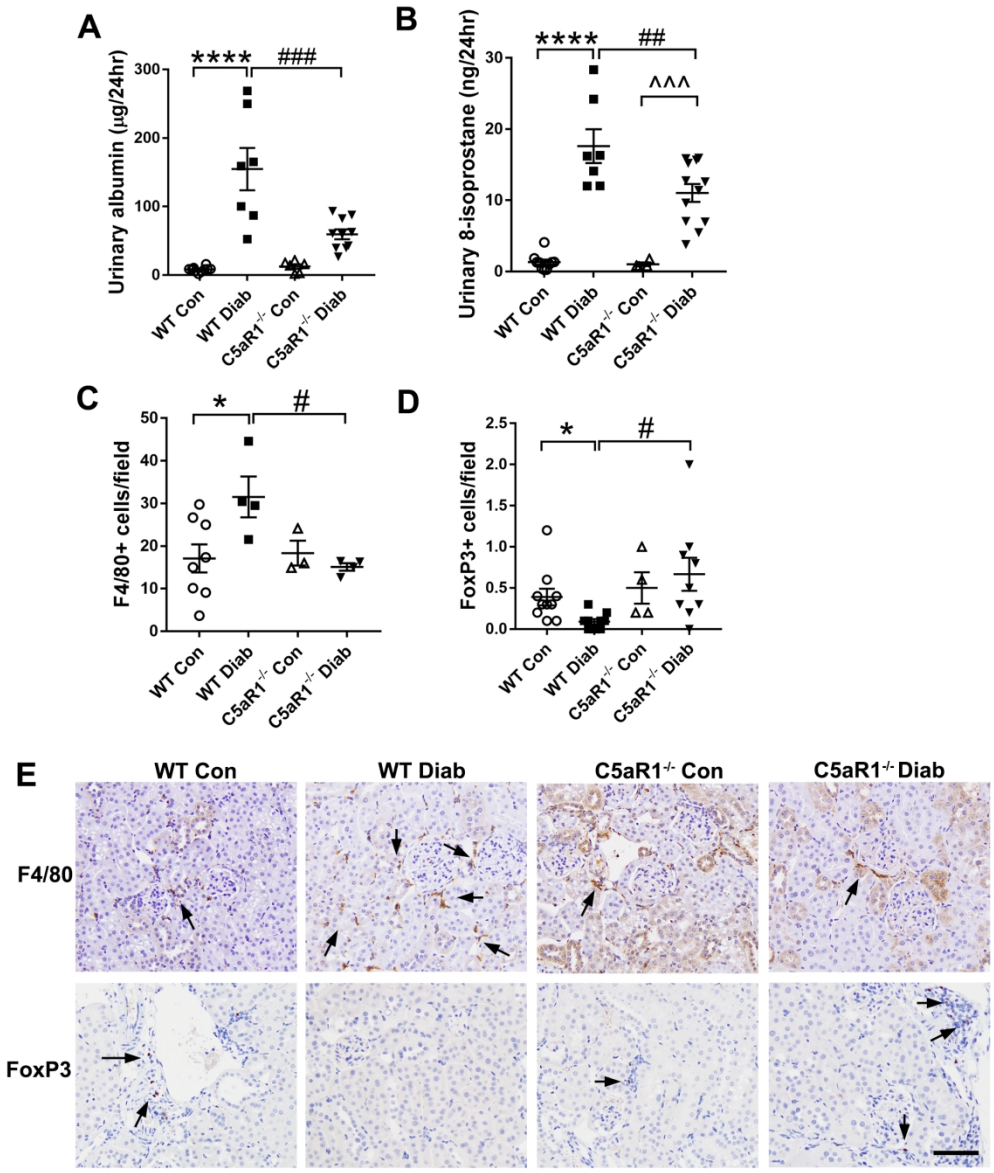

Figure 3. Genetic deletion of C5aR1 protects against diabetes-induced inflammation and renal injury. Urinary albumin (A) and 8-isoprostane (B) were determined in wildtype control and diabetic mice and in C5aR1-/- control and diabetic mice. (C) F4/80+ cells in the renal cortex (C, E top row). (D) FoxP3+ cells the renal cortex (D, E bottom row). Original magnification ×200. Scale bar = 50µm. n = 4-12 mice/group. *P<0.05, **P<0.01, ****P<0.0001 vs WT Con; #P<0.05, ##P<0.01, ###P<0.001 vs WT Diab; ^^^P<0.001 vs C5aR1-/- Con. The line within the scatterplot represents the mean.

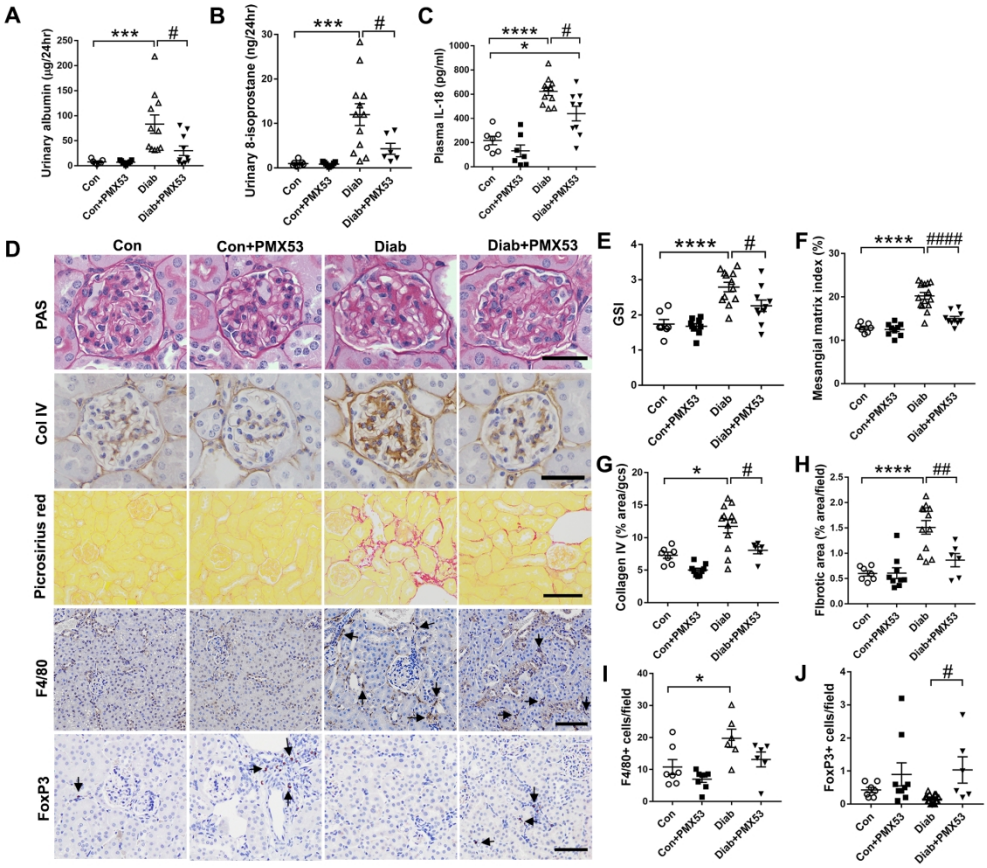

Figure 4. C5aR1 inhibition by PMX53 is efficacious in DKD. Wildtype control and STZ-diabetic mice were treated with 2mg/kg/day PMX53 for 24 weeks and urinary albumin (A) 8-isoprostane (B) and plasma IL-18 (C) were determined. Renal histology was examined by staining paraffin-embedded sections with Periodic acid-Schiff (PAS) and glomerulosclerotic index (D, E) and mesangial matrix expansion (D, F) was quantitated. Glomerular Collagen IV deposition was determined (D, G). Kidney fibrotic area was determined by picrorsirius red staining (D, H). Inflammatory F4/80+ cells (D, I) and anti-inflammatory FoxP3+ cells (D, J) in the kidney were examined by immunohistochemistry. Original magnification ×400 and scale bar = 25μm for PAS and Col IV. Original magnification ×200 and scale bar = 50μm for picrosirius red, F4/80 and FoxP3. n = 6-12 mice/group. *P<0.05, ***P<0.001, ****P<0.0001 vs Con; #P<0.05, ##P<0.01, ####P<0.0001 vs Diab. The line within the scatterplot represents the mean.

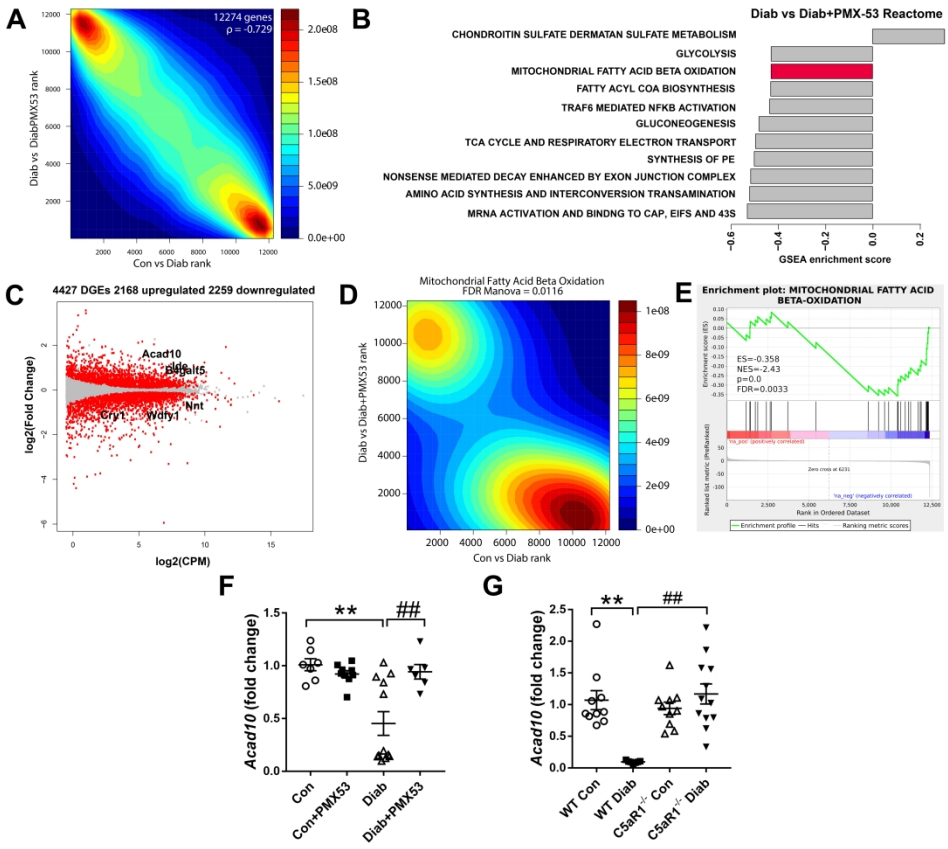

Figure 5. RNA-Seq analysis reveals a role for C5aR1 in pathways involved in mitochondrial fatty acid beta-oxidation. (A) Rank-rank density plot of differential gene expression due to diabetes and PMX53 treatment. (B) GSEA analysis of diabetes vs diabetes+PMX53 showing the top REACTOME pathways, with mitochondrial fatty acid beta-oxidation pathway highlighted red. (C) MA plot of top differential genes in diabetes vs diabetes+PMX53 groups with the top three downregulated and top three upregulated genes highlighted. (D) Rank-rank density plot of differential genes in the mitochondrial fatty acid beta-oxidation pathway. (E) Gene set enrichment analysis highlighted genes that were altered by PMX53 in the mitochondrial fatty acid beta-oxidation pathway in diabetic mice. (F) Acad10 expression in PMX53 treated mice and (G) C5aR1-/- mice. mice/group. n = 6-12, **P<0.01 vs Con or WT Con, ##P<0.01 vs Diab or WT Diab. The line within the scatterplot represents the mean.

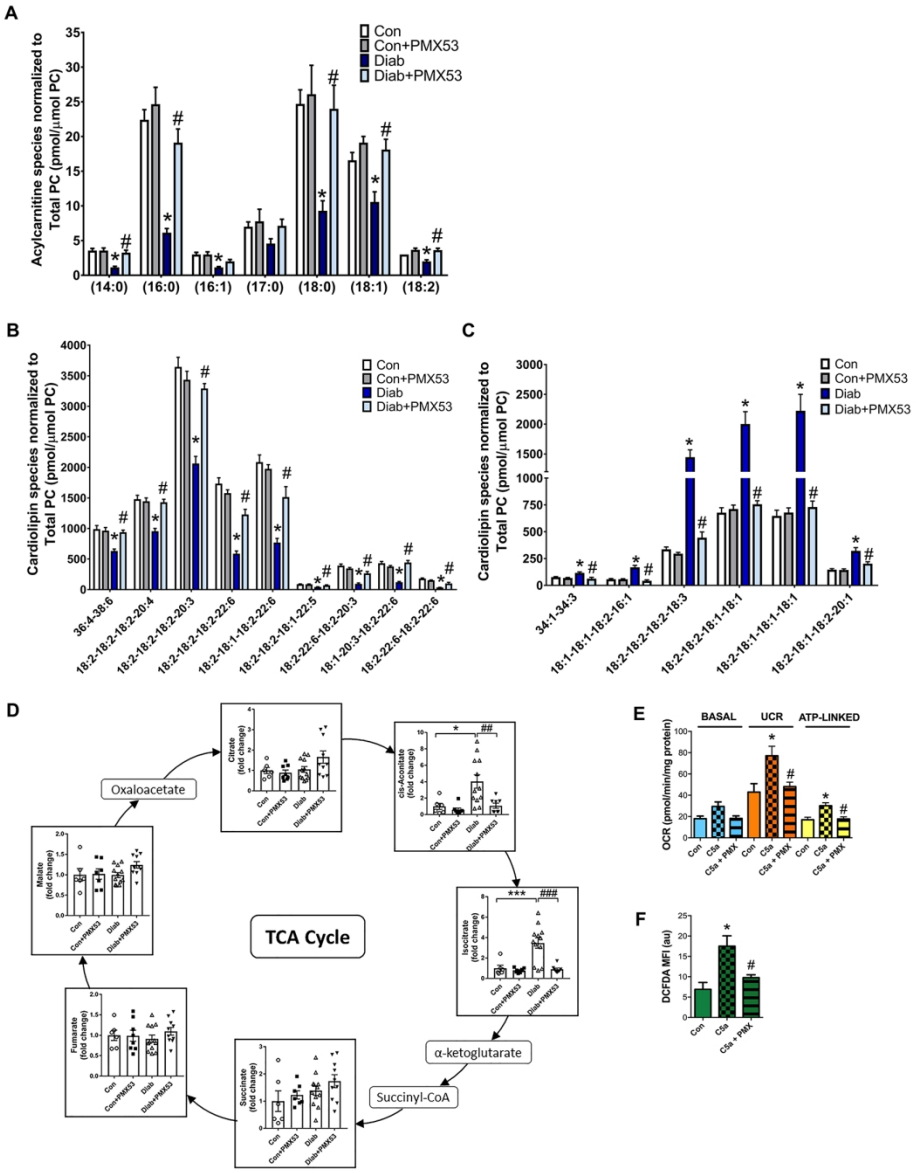

Figure 6. Diabetes induces changes to mitochondrial agility including kidney cardiolipin remodelling and enhanced TCA cycle intermediate generation, which are normalised by C5aR1 inhibition. Lipidomics of renal cortex was performed to determine (A) Acylcarnitine species and (B) Cardiolipin species that were downregulated in diabetes and restored by PMX53 treatment, or (C) Cardiolipin species that were upregulated in diabetes and attenuated by PMX53 treatment. Data are mean±SEM, n=6-12 mice/group. (D) TCA cycle intermediates in renal cortex were determined by metabolomics, n=6-12 mice/group. *P<0.05, ***P<0.001 vs Con, #P<0.05, ##P<0.01, ###P<0.001 vs Diab. (E) Human primary proximal tubule epithelial cells (PTECs) were exposed to C5a or C5a plus PMX53 for 24 hours and mitochondrial oxygen consumption rate (OCR), including basal, carbonyl cyanide-4-(trifluoromethoxy) phenylhydrazone (FCCP)-uncoupled (UCR), and ATP-linked respiration was determined by Seahorse Flux Analyzer. Values are mean±SEM, n≥9 replicates per group. *P<0.05 vs Con, #P<0.05 vs C5a-treated cells. (F) PTECs were exposed to C5a or C5a plus PMX53 for 24 hours and reactive oxygen species production was determined using the DCFDA probe with flow cytometry detection. Values are mean±SEM, n=3 replicates per group. *P<0.05 vs Con, #P<0.05 vs C5a-treated cells.

Tan SM et al.,

Online Supplementary Materials

Method for PMX53 Pharmacokinetics

C57BL/6 J mice (males, 10–12 weeks old) were purchased from Animal Resources Centre, Western Australia. After overnight fasting, mice ($n = 4$ per time point) were anaesthetized with zolazapam (50 mg/kg) and xylazine (12 mg/kg) via *i.p*. injection. Anaesthetized mice were administered 1 mg/kg of PMX53 in 5% dextrose water for injection either through the tail vein for intravenous route (*i.v.*) or by oral gavage for per-oral route (*p.o.*). Blood samples were collected from separate mice via cardiac puncture at 2.5 min, 5 min, 10 min, 15 min, 30 min, 45 min, 60 min and 90 minutes in tubes containing EDTA followed by plasma separation by centrifugation at 1500 × *g* at 4 °C. Plasma samples were stored at -80 °C for further processing and analysis. On the day of analysis, 50 µl of plasma was mixed with 10 µl of 1 µg/ml of internal standard (PMX205) and processed for quantitative analysis of PMX53 using a validated LC-MS/MS method [71]. Pharmacokinetic data analysis was performed using Pharsight WINNONLIN software (version 6.4) to obtain various pharmacokinetic parameters along with PMX53 bioavailability determination.

Method for the Measurement of Polar Acylcarnitines

Analysis of polar acylcarnitines was done using HILIC chromatography in conjunction with an Agilent 6490 QQQ mass spectrometer. Solvent A contains 95% acetonitrile, 5% water, 10mM ammonium formate and 0.1% formic acid while solvent B comprising of 50% acetonitrile, 50% water, 10mM ammonium formate and 0.1% formic acid. Separation was performed at a flow rate of 0.4ml/minute on an InfinityLab Poroshell 120 HILIC-Z column (2.1 x 100 mm, 2.7 µm) with the following conditions; Solvent B starting at 0%, holding

isocratic for 1 minute before ramping to 100% solvent B over 5 minutes. The method was held at 100% B for 1 minute before returning to 0% B over 0.1 minutes. The column was then equilibrated with 0% B for 5.9 minutes for a total run time of 13 minutes.

Supplementary Figures

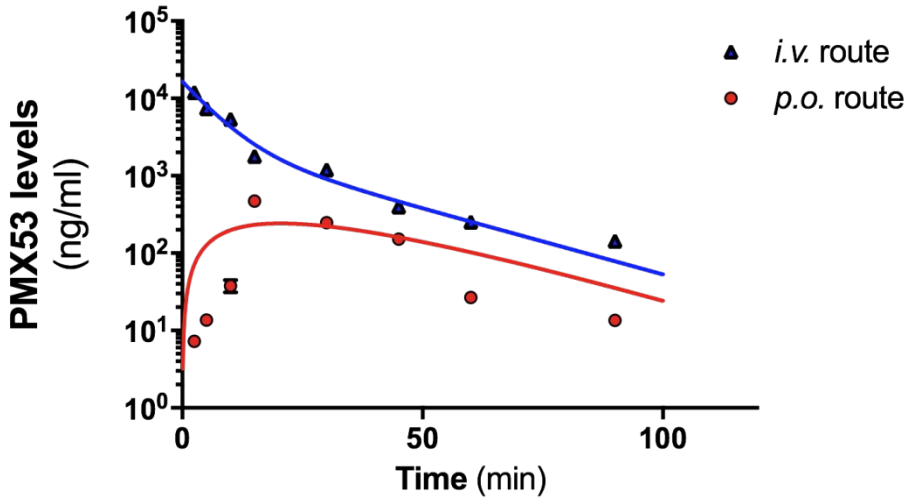

Fig. S1. Pharmacokinetic determination of PMX53 plasma concentrations in mice. C57Bl/6J mice were injected intravenously (i.v.) or by oral gavage (p.o.) with PMX53 (1mg/kg), and blood collected from separate mice at various time points up to 90 minutes post-injection. Data points represent individual values (mean±SEM; n=4 mice), and lines represent predicted values using two-compartmental analysis.

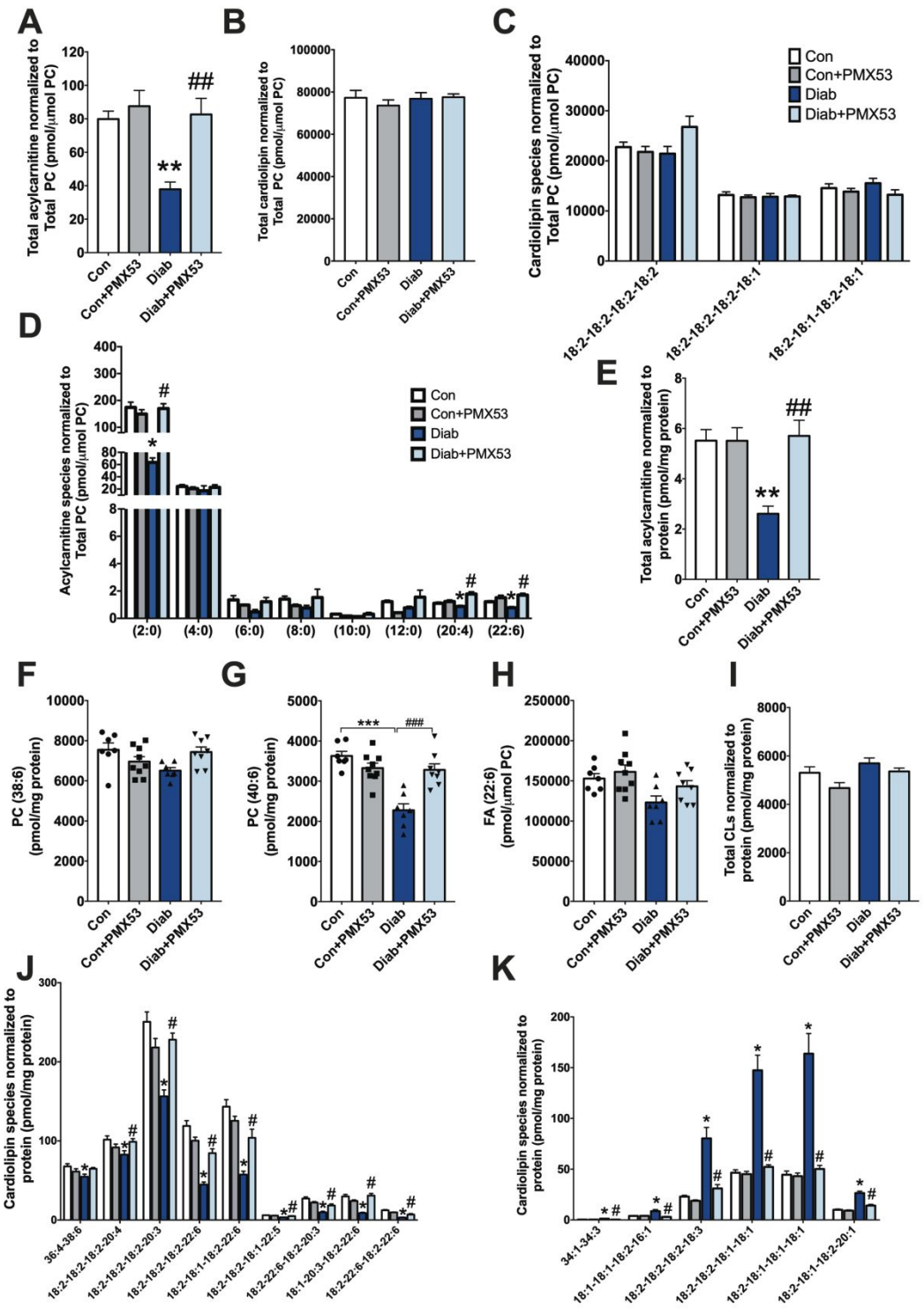

Fig. S2. Profile of acylcarnitine, cardiolipin and other lipid species in renal cortex.

(A) Total acylcarnitine levels in the renal cortex. (B) Total cardiolipin levels in the renal cortex. (C) Abundant cardiolipin species in the renal cortex not altered by diabetes and/or PMX53 treatment. (D) Short and long chain acylcarnitines were detected by HILIC method.

(E) Total acylcarnitine levels in the renal cortex normalized to total protein. (F) PC(38:6), (G) PC(40:6) and (H) Free fatty acid (22:6) were also measured. Cardiolipin species normalized to total protein: (I) total cardiolipins, (J) downregulated cardiolipin species, (K) upregulated cardiolipin species. Data are mean±SEM, n=6-12 mice/group. *P<0.05, **P<0.01 vs Con, #P<0.05, ##P<0.01 vs Diab.

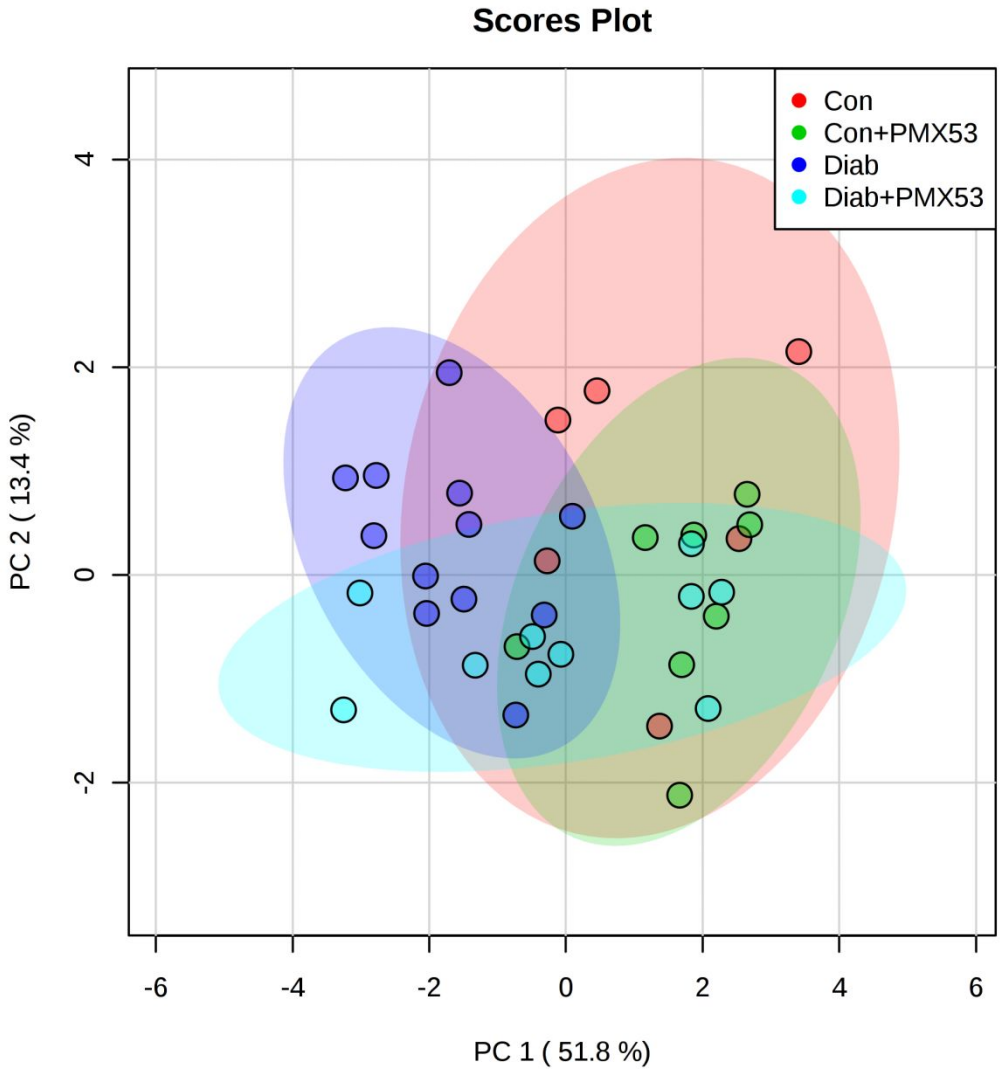

Fig. S3. Metabolomic analyses of kidney cortex.

PCA plot and showing TCA cycle metabolites in renal cortex from control and streptozotocin-induced diabetic C57BL/6 mice treated with or without PMX53.

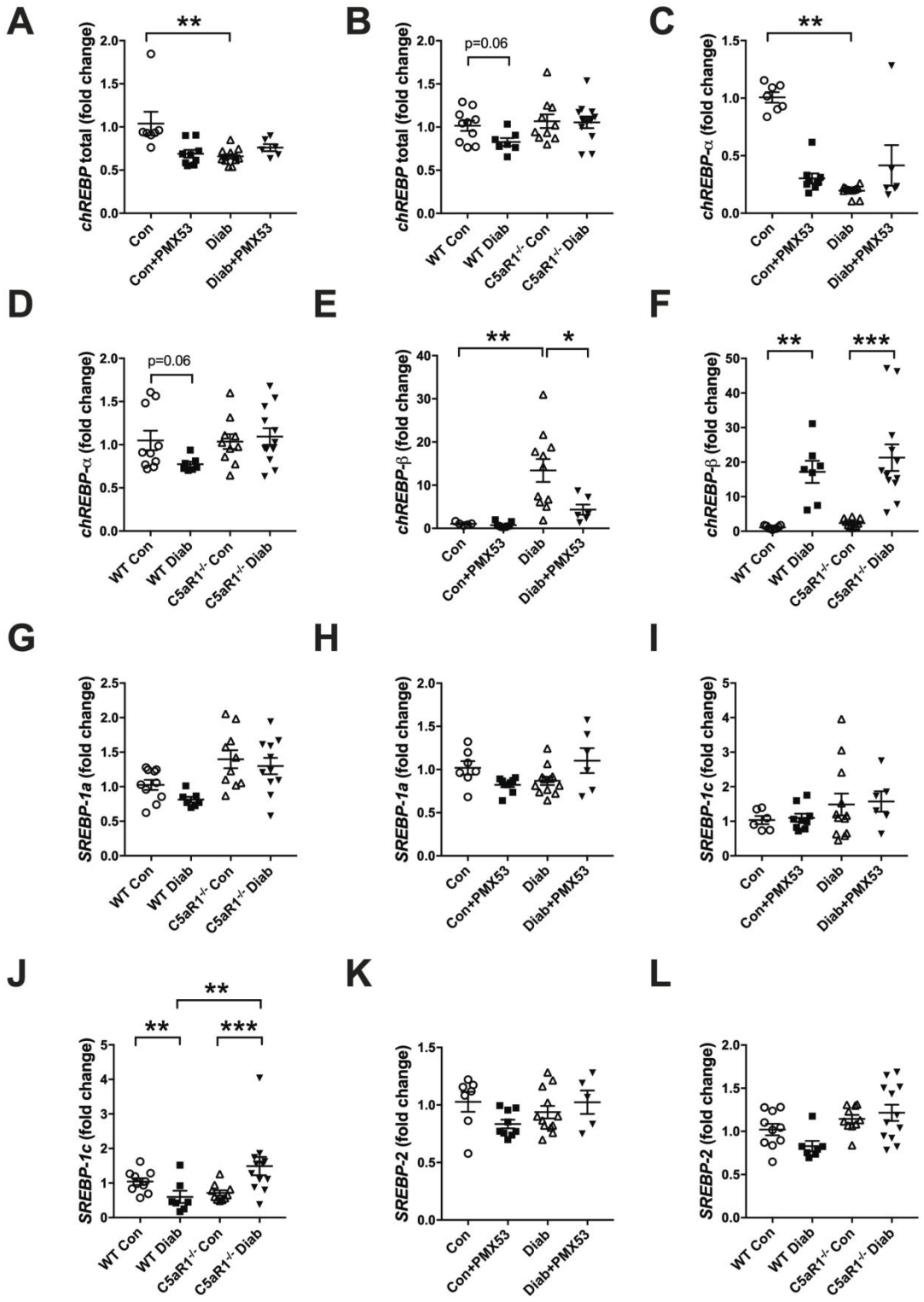

Fig. S4. Renal cortical gene expression of transcription factors involved in fatty acid synthesis. (A) Total chREBP in control and diabetic mice with or without PMX53 treatment.

(B) Total chREBP in control and diabetic mice with C5aR1 genetic deletion. (C) chREBP-alpha in control and diabetic mice with or without PMX53 treatment. (D) chREBP-alpha in control and diabetic mice with C5aR1 genetic deletion. (E) chREBP-beta in control and diabetic mice with or without PMX53 treatment. (F) chREBP-beta in control and diabetic mice with C5aR1 genetic deletion. (G) SREBP-1a in control and diabetic mice with or without PMX53 treatment. (H) SREBP-1a in control and diabetic mice with C5aR1 genetic deletion. (I) SREBP-1c in control and diabetic mice with or without PMX53 treatment. (J) SREBP-1c in control and diabetic mice with C5aR1 genetic deletion. (K) SREBP-2 in control and diabetic mice with or without PMX53 treatment. (L) SREBP-2 in control and diabetic mice with C5aR1 genetic deletion. Data are mean±SEM, n=6-12 mice/group. *P<0.05, **P<0.01, ***P<0.001.

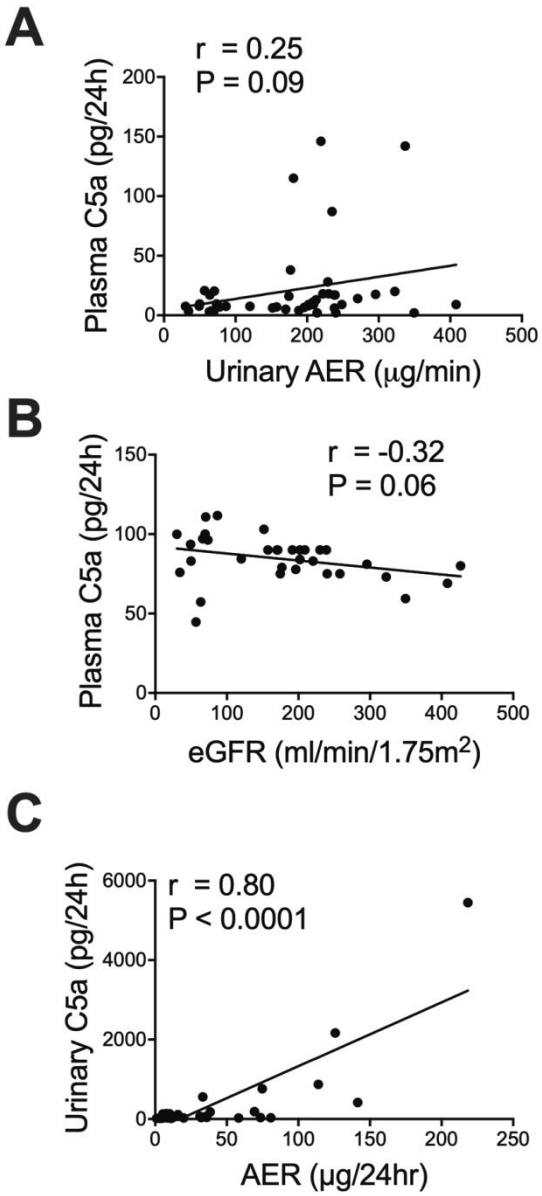

Fig. S5. Correlation analyses of C5a and albuminuria or eGFR in the setting of diabetes. Pearson's correlation analysis was used to determine the relationship between: (A) plasma C5a and urine albumin in human diabetes, (B) plasma C5a and eGFR in human diabetes, (C) urinary C5a and urinary albumin in the STZ mouse model of diabetes.

Supplementary Tables

Table S1. Clinical characteristics of participants from which plasma was obtained for complement measurement.

	Control (n=38)	Type 1 diabetes (n=18)	Type 2 diabetes (n=20)	Type 1 diabetes + RAS (n=19)	Type 2 diabetes + RAS (n=20)
Gender (M/F)	15/23	10/8	11/9	14/5	13/7
Age (years)	46±11	40±15	63±9	63±13	68±10
eGFR (ml/min/1.73m^2)	NA	83±8	74±18	71±15	70±20
Urinary albumin (μg/min)	NA	8±6	20±45	87±260	45±88

Data are mean±SD.

Table S2. PMX53 pharmacokinetic parameters.

Parameters*	**Units**	***p.o.* route**	***i.v.* route**
Tmax	min	20.32	---
Cmax	μg/mL	0.24	17.42
Alpha_HL	min	14.04	3.49
Beta_HL	min	22.89	14.73
MRTlast	min	28.00	13.21
MRTINF_obs	min	29.83	18.03
MRTINF_pred	min	29.90	17.92
AUC	(min*μg/ml)	11.78	204.63
Bioavailability	%	5.7	100

*where Tmax represents time corresponding to max plasma conc. of PMX53; C max, max concentration of PMX53; Alpha HL represents distribution half-life; Beta HL represents

elimination half-life; MRT, mean residence time; and AUC is area under the concentration-time curve from time zero to time t i.e. 90 min.

Table S3. Kidney cortex mRNA expression of genes involved in mitochondrial fatty acid β-oxidation and fatty acid metabolism in streptozotocin-induced diabetic mice treated with or without PMX53.

Pathway	Gene Name	Gene Symbol	Log2 Fold Change	FDR
Mitochondrial fatty acid β-oxidation	Enoyl-Coenzyme A delta isomerase 1	***Eci1***	**-0.5348**	**3.33E-08**
	hydroxyacyl-CoA dehydrogenase trifunctional multienzyme complex subunit alpha	***Hadha***	**-0.33607**	**8.32E-07**
	Acyl-CoA dehydrogenase, long chain	***Acadl***	**-0.18593**	**0.000101**
	Methylmalonyl CoA epimerase	***Mcee***	**-0.14891**	**0.000576**
	Propionyl-CoA carboxylase subunit alpha	***Pcca***	**0.167554**	**0.010026**
	Acyl-Coenzyme A dehydrogenase, very long chain	***Acadvl***	**-0.15296**	**0.010206**
	2,4-dienoyl CoA reductase 1, mitochondrial	***Decr1***	**-0.2117**	**0.018426**
	Propionyl Coenzyme A carboxylase, beta polypeptide	***Pccb***	**0.142277**	**0.018636**
	Acyl-Coenzyme A dehydrogenase, medium chain	***Acadm***	**-0.16853**	**0.035528**
	Acyl-Coenzyme A dehydrogenase, short chain	*Acads*	0.223574	0.051019
	Methylmalonyl-Coenzyme A mutase	*Mut*	0.086252	0.165725
	Enoyl Coenzyme A hydratase, short chain, 1, mitochondrial	*Echs1*	-0.07282	0.169622
	Hydroxyacyl-Coenzyme A dehydrogenase	*Hadh*	0.024264	0.801194
Fatty acid metabolism	Enoyl-Coenzyme A delta isomerase 1	***Eci1***	**-0.5348**	**3.33E-08**
	Acetyl-Coenzyme A acetyltransferase 1	***Acat1***	**0.257547**	**0.006373**
	Acyl-CoA synthase	*Acss2*	0.182849	0.132779
	Acetyl-Coenzyme A carboxylase alpha	*Acaca*	0.124141	0.206389
	Methylmalonyl-Coenzyme A mutase	*Mut*	0.086252	0.165725
	Catalase	*Cat*	0.079878	0.274439
	Carnitine palmitoyltransferase 1c	*Cpt1c*	-0.10544	0.467711
	Fatty acid synthase	*Fasn*	-0.0415	0.684343
	Carnitine palmitoyltransferase 1a	*Cpt1a*	-0.03072	0.774633
	Hydroxyacyl-Coenzyme A dehydrogenase	*Hadh*	0.024264	0.801194

	Enoyl-Coenzyme A, hydratase/3-hydroxyacyl Coenzyme A dehydrogenase	*Ehhadh*	-0.02053	0.916932

Log2 Fold Change is Diab vs Diab+PMX53. Significance was defined as FDR < 0.05.

Table S4. Raw data of lipid species determined in the kidney of streptozotocin-induced diabetic mice treated with or without PMX53.

Lipid species	Con (n=7)	Con+PMX53 (n=9)	Diab (n=7)	Diab+PMX53 (n=8)	ANOVA p value (BH)
AC(14:0)	3.5±0.3	3.6±0.4	1.2±0.1	3.2±0.4	**7.64E-05**
AC(16:0)	22.5±1.4	24.8±2.4	6.2±0.6	19.1±1.9	**4.14E-06**
AC(16:1)	2.8±0.3	3.0±0.3	1.1±0.1	2.1±0.2	**2.19E-04**
AC(17:0)	6.9±0.6	7.8±1.7	4.7±0.7	7.3±1.0	3.60E-01
AC(18:0)	24.5±2.0	26.1±4.2	9.2±1.4	29.1±6.0	**1.96E-02**
AC(18:1)	16.6±1.2	19.0±0.9	10.9±1.5	18.1±1.5	**1.34E-03**
AC(18:2)	3.0±0.1	3.5±0.2	2.0±0.2	3.7±0.3	**2.86E-04**
PC(28:0)	77.3±7.8	79.3±7.3	73.3±3.1	58.8±8.8	2.47E-01
PC(14:0_16:0)	6897±228	6796±204	5135±333	5686±606	**1.32E-02**
PC(31:1)	129±8.0	147±9.6	252±27.7	129±9.1	**3.03E-05**
PC(31:0)	3470±141	3740±157	3799±208	4278±265	8.63E-02
PC(32:2)	721±33.0	792±34.3	1248±129	640±60.3	**3.96E-05**
PC(32:1)	10700±294	11244±503	11796±1079	8282±1246	5.88E-02
PC(16:0_16:0)	168486±2796	167850±1659	113272±7177	152330±4672	**2.68E-08**
PC(33:2)	745±37.7	811±36.3	1205±70.9	1027±108	**8.56E-04**
PC(33:1)	2315±62.3	2479±97.8	3044±111	2496±83.5	**2.13E-04**
PC(33:0)	2654±107	2877±138	3104±140	3332±259	9.21E-02
PC(34:5)	21.9±1.0	22.5±0.9	89.8±11.5	23.1±1.2	**1.00E-08**
PC(14:0_20:4)	180±11.4	192±10.9	353±38.6	178±12.8	**1.39E-05**
PC(16:1_18:2)\PC(16:0_18:3)	7957±186	8117±327	20599±1089	8197±316	**1.64E-13**
PC(16:0_18:2)	120391±3666	117904±3463	107515±3279	118445±4594	1.63E-01
PC(16:0_18:1)	120404±1489	124024±1546	157115±2766	123310±4093	**1.00E-08**
PC(16:0_18:0)	19012±450	18172±244	20179±463	19305±449	**1.93E-02**
PC(35:5)	27.2±1.5	28.1±1.0	69.1±6.9	31.9±1.8	**2.68E-08**
PC(15:0_20:4)	354±23.0	382±19.7	312±23.3	440±34.1	**2.20E-02**
PC(35:3)	384±15.9	409±12.6	536±24.5	431±20.9	**1.07E-04**
PC(35:2)	1484±49.9	1611±41.7	2351±78.3	2084±218	**2.79E-04**
PC(35:1)	418±19.6	444±15.8	447±22.3	425±15.9	6.51E-01
PC(36:6)	758±49.0	749±26.9	764±45.5	616±71.8	1.79E-01
PC(36:5)	7192±473	6943±513	9969±882	6527±590	**5.57E-03**
PC(18:2_18:2)\PC(16:0_20_4)	83721±2868	82334±2782	52537±469	84246±1671	**3.90E-09**
PC(36:2)	74881±1760	72943±2638	140753±7353	83607±4433	**1.08E-09**
PC(18:0_18:1)	8795±225	8978±203	9091±405	9084±187	8.57E-01
PC(36:0)	389±9.0	406±14.5	548±15.0	445±15.1	**4.61E-07**
PC(15:0_22:6)	1240±69.3	1338±76.6	1377±62.9	1488±102	2.71E-01
PC(15-MHDA_20:4)\PC(17:0_20:4)	2163±71.2	2279±65.7	1524±71.4	2682±199	**1.93E-05**

Lipid species	Con (n=7)	Con+PMX53 (n=9)	Diab (n=7)	Diab+PMX53 (n=8)	ANOVA p value (BH)
PC(38:7)	7299±269	6806±176	7542±334	5342±444	**4.44E-04**
PC(38:6)	109692±3864	110430±5197	88374±1999	107436±2748	**2.91E-03**
PC(38:5)	44948±762	46752±616	54652±1323	48533±1379	**2.78E-05**
PC(38:4)	63917±1300	65409±1590	53907±1898	76520±2374	**4.90E-07**
PC(18:0_20:3)	6589±261	6119±157	7751±403	5930±158	**2.79E-04**
PC(38:2)	21882±532	21199±416	25802±1037	20536±526	**6.28E-05**
PC(39:6)	4224±219	4500±226	2959±253	4905±393	**1.09E-03**
PC(39:5)	664±47.3	601±15.9	659±32.1	623±29.2	4.76E-01
PC(40:10)	50.9±2.7	46.6±3.2	91.1±8.9	41.7±3.3	**2.38E-06**
PC(40:8)	13154±489	12633±174	15369±798	14185±716	**1.90E-02**
PC(40:7)	20242±574	20151±205	33224±2434	19655±547	**6.99E-08**
PC(18:0_22:6)	52798±1149	52445±1361	30893±2212	47317±1522	**8.37E-09**
PC(18:0_22:5)	6240±154	6496±146	7492±315	6399±266	**6.52E-03**
PC(18:0_22:4)\PC(20:0_20:4)	1764±27.8	1847±41.3	1396±111	2102±88.7	**2.11E-05**
PC(44:12)	570±27.3	474±10.4	833±58.8	652±52.4	**3.59E-05**
TG(48:0) [NL-16:0]	6087±520	5912±410	1785±144	4202±659	**1.41E-05**
TG(48:0) [NL-18:0]	313±24.9	331±24.2	221±12.9	280±12.2	**6.70E-03**
TG(48:1) [NL-16:1]	1577±214	1583±143	796±53.5	1080±100	**1.83E-03**
TG(48:1) [NL-18:1]	1424±196	1377±113	696±75.0	938±119	**2.61E-03**
TG(48:2) [NL-14:0]	818±129	835±117	276±39.1	557±156	**1.90E-02**
TG(48:2) [NL-14:1]	180±30.3	204±26.6	240±65.6	133±9.9	2.85E-01
TG(48:2) [NL-16:1]	1589±252	1662±164	1132±85.3	1215±62.2	7.91E-02
TG(48:2) [NL-18:2]	894±123	860±73.5	264±34.5	572±140	**1.39E-03**
TG(48:3) [NL-14:0]	143±34.2	142±22.7	75.6±18.7	87.4±29.7	2.38E-01
TG(48:3) [NL-16:1]	569±90.1	609±60.4	468±50.1	462±26.8	2.70E-01
TG(48:3) [NL-18:3]	83.3±15.9	78.5±7.7	59.0±13.4	51.5±15.8	3.30E-01
TG(48:3) [SIM]	1031±164	1111±123	856±170	782±99.9	3.46E-01
TG(49:1) [NL-16:1]	281±21.2	321±43.4	250±14.4	282±19.7	4.55E-01
TG(50:0) [NL-18:0]	445±64.6	423±32.7	216±16.4	345±24.8	**2.49E-03**
TG(50:1) [NL-18:1]	5380±893	4416±664	1698±257	3412±582	**7.96E-03**
TG(50:2) [NL-18:2]	3527±432	3193±322	656±116	2162±395	**5.93E-05**
TG(50:3) [NL-18:3]	499±63.1	447±47.5	229±54.0	284±71.1	**1.88E-02**
TG(50:4) [NL-20:4]	119±29.6	109±18.9	19.2±4.0	56.4±5.7	**3.07E-03**
TG(51:0) [SIM]	2638±624	2229±224	1525±183	1966±176	2.22E-01
TG(54:0) [NL-18:0]	179±9.9	191±13.1	163±6.7	183±5.8	3.09E-01
TG(54:1) [NL-18:1]	91.5±12.4	92.6±9.2	60.4±5.3	76.2±9.3	1.12E-01
TG(54:1) [SIM]	449±39.1	473±40.1	335±21.9	408±32.1	7.91E-02
TG(54:2) [NL-18:0]	1174±190	1355±235	773±109	1591±640	5.30E-01
TG(54:3) [SIM]	2793±684	2866±619	1738±274	2520±632	5.73E-01
TG(54:4) [NL-18:2]	533±112	521±94.7	322±41.7	570±195	5.73E-01
TG(56:6) [NL-22:5](a)	145±26.7	134±18.1	63.9±14.4	86.6±12.8	**2.33E-02**
TG(56:6) [NL-22:5](b)	145±26.7	134±18.1	63.9±14.4	86.6±12.8	**2.33E-02**
TG(56:6) [SIM]	2483±317	2270±184	1548±318	1798±263	1.15E-01
TG(56:7) [NL-20:4]	873±127	1169±213	789±240	1142±460	7.60E-01
TG(56:7) [SIM]	5550±796	4573±498	3288±804	3162±446	6.66E-02
TG(56:8) [NL-20:4]	214±36.1	227±22.7	152±47.1	216±72.4	7.25E-01
TG(56:9) [NL-22:6]	152±40.6	114±18.9	180±70.7	72.2±12.9	3.04E-01
TG(58:10) [NL-22:6]	489±77.9	383±43.3	381±138	291±41.8	4.40E-01
TG(58:8) [NL-22:6]	353±68.8	270±20.6	361±121	237±40.7	5.33E-01
TG(58:9) [NL-22:6]	479±97.8	346±29.8	367±132	297±68.0	5.33E-01
Ubiquinone	235066±14941	204603±12997	158334±4738	199733±13708	**6.77E-03**
CL 34:1_32:2	51.3±4.5	46.7±3.7	53.5±7.2	36.5±8.4	2.92E-01
CL 34:1_34:4	4.5±1.0	4.8±1.1	23.8±1.8	4.6±0.7	**1.23E-10**
CL 34:1_34:3	77.2±4.1	68.6±4.9	115±10.1	62.4±12.4	**2.01E-03**

Lipid species	Con (n=7)	Con+PMX53 (n=9)	Diab (n=7)	Diab+PMX53 (n=8)	ANOVA p value (BH)
CL 34:1_34:1	1941±114	1807±76.9	1314±87.1	1744±186	**1.99E-02**
CL 18:2_18:2_18:2_16:1	1885±120	1823±82.2	1253±111	1193±224	**4.32E-03**
CL 18:2_18:2_18:1_16:1	1147±71.0	1095±55.7	996±60.1	914±113	2.38E-01
CL 18:2_18:1_18:2_16:1	1113±83.4	1053±57.8	1011±93.0	713±172	9.68E-02
CL 18:1_18:1_18:2_16:1	57.4±6.4	57.0±4.4	168±18.3	43.2±8.5	**5.24E-08**
CL 18:2_18:1_18:1_16:1	1454±97.5	1336±68.1	1409±73.4	1129±163	2.35E-01
CL 18:2_18:2_18:2_18:3	336±21.8	296±11.7	1445±125	445±53.0	**5.71E-11**
CL 18:2_18:2_18:2_18:2	22750±994	21794±1103	21434±1454	26787±2138	8.95E-02
CL 18:2_18:2_18:2_18:1	13190±627	12734±451	12824±663	12887±290	9.32E-01
CL 18:2_18:2_18:1_18:1	678±46.1	712±37.1	2003±206	757±32.8	**8.37E-09**
CL 18:2_18:1_18:2_18:1	14559±854	13854±645	15539±971	13226±1005	3.47E-01
CL 18:2_18:1_18:1_18:1	648±52.8	679±44.0	2225±275	730±56.7	**4.31E-08**
CL 18:2_16:1_18:2_22:6	107±9.1	105±7.5	45.8±6.7	60.3±17.8	**2.10E-03**
CL 18:2_18:2_16:1_22:6	101±10.1	103±8.9	128±7.4	79.6±8.9	**1.70E-02**
CL 36:4_38:6	991±56.9	966±50.0	630±33.4	940±33.7	**6.28E-05**
CL 18:2_18:2_18:2_20:4	1479±64.4	1446±53.8	955±46.1	1430±47.6	**2.38E-06**
CL 18:2_18:2_18:2_20:3	3646±156	3435±138	2063±116	3291±80.4	**8.72E-08**
CL 18:2_18:1_18:2_20:3	1651±104	1533±81.8	1278±76.7	1441±90.5	7.91E-02
CL 18:2_18:2_18:1_20:3	1544±77.8	1389±65.9	988±58.5	2554±385	**2.86E-04**
CL 18:2_18:2_18:1_20:2	199±11.2	197±9.9	356±20.7	338±45.2	**2.33E-04**
CL 18:2_18:1_18:2_20:2	1221±71.3	1121±59.5	1020±67.0	1839±167	**6.28E-05**
CL 18:2_18:2_18:1_20:1	9.8±1.4	6.6±1.2	33.5±3.8	17.0±2.3	**2.25E-07**
CL 18:2_18:1_18:2_20:1	146±9.9	144±9.4	322±30.4	204±17.5	**1.87E-06**
CL 18:2_18:2_18:2_22:6	1734±96.2	1579±53.5	588±43.4	1228±85.7	**2.23E-09**
CL 18:2_18:2_18:1_22:6	521±35.7	457±16.1	338±16.3	402±23.8	**3.03E-04**
CL 18:2_18:1_18:2_22:6	2085±118	1977±67.7	770±66.9	1514±171	**2.98E-07**
CL 18:2_18:1_18:2_22:5	581±33.7	539±17.2	405±22.6	464±47.1	**7.26E-03**
CL 18:2_18:2_18:1_22:5	87.8±4.3	86.9±4.1	41.8±4.4	70.9±7.1	**1.39E-05**
CL 18:2_18:2_20:3_22:6	61.7±8.3	47.5±4.2	12.3±4.4	30.5±5.6	**6.09E-05**
CL 18:2_22:6_18:2_20:3	393±24.8	347±14.3	92.8±15.2	266±29.5	**2.65E-08**
CL 20:3_22:6_18:2_18:1	75.4±8.9	69.7±10.1	20.7±1.4	49.1±14.0	**7.62E-03**
CL 18:1_20:3_18:2_22:6	431±29.2	379±14.9	120±12.5	443±33.5	**1.45E-08**
CL 18:1_22:6_18:2_20:3	138±13.5	130±8.1	66.8±4.6	97.5±10.7	**2.39E-04**
CL 18:2_18:2_22:6_22:6	8.7±2.5	6.3±1.7	1.8±0.7	5.5±1.3	8.95E-02
CL 18:2_22:6_18:2_22:6	179±11.4	152±6.2	34.9±2.8	100±18.3	**9.72E-08**
AC(2:0)	174±19.6	149±16.1	63.5±7.4	170±18.0	**5.32E-04**
AC(4:0)	24.2±3.0	20.7±2.8	17.2±8.1	22.8±4.1	7.79E-01
AC(6:0)	1.3±0.3	1.0±0.1	0.5±0.2	1.2±0.3	9.34E-02
AC(8:0)	1.4±0.2	0.9±0.1	0.8±0.2	1.5±0.6	3.99E-01
AC(10:0)	0.3±0.0	0.2±0.0	0.1±0.0	0.3±0.1	2.50E-01
AC(12:0)	1.2±0.1	1.0±0.1	0.8±0.1	1.6±0.5	3.04E-01
AC(20:4)	1.1±0.1	1.2±0.1	0.9±0.1	1.8±0.2	**3.69E-04**
AC(22:6)	1.2±0.1	1.5±0.2	0.8±0.1	1.7±0.1	**8.50E-04**

Data are mean±SEM. p-values corrected for multiple comparisons by the method of Benjamini and Hochberg. Significant corrected p-values (<0.05) shown in bold.